



OPEN ACCESS

Original research

# PI3K-driven HER2 expression is a potential therapeutic target in colorectal cancer stem cells

Laura Rosa Mangiapane,<sup>1</sup> Annalisa Nicotra,<sup>1</sup> Alice Turdo ,<sup>2</sup> Miriam Gaggianesi,<sup>1</sup> Paola Bianca,<sup>1</sup> Simone Di Franco,<sup>1</sup> Davide Stefano Sardina,<sup>1</sup> Veronica Veschi,<sup>1</sup> Michele Signore ,<sup>3</sup> Sven Beyes,<sup>4</sup> Luca Fagnocchi ,<sup>4</sup> Micol Eleonora Fiori ,<sup>5</sup> Maria Rita Bongiorno,<sup>2</sup> Melania Lo Iacono,<sup>1</sup> Irene Pillitteri,<sup>1</sup> Gloria Ganduscio,<sup>1</sup> Gaspare Gulotta,<sup>1</sup> Jan Paul Medema,<sup>6,7</sup> Alessio Zippo,<sup>4</sup> Matilde Todaro,<sup>2</sup> Ruggero De Maria,<sup>8,9</sup> Giorgio Stassi <sup>1</sup>

► Additional material is published online only. To view, please visit the journal online (<http://dx.doi.org/10.1136/gutjnl-2020-323553>).

For numbered affiliations see end of article.

## Correspondence to

Professor Giorgio Stassi, Department of Surgical, Oncological and Stomatological Sciences, Università degli Studi di Palermo, Palermo, Italy; [giorgio.stassi@unipa.it](mailto:giorgio.stassi@unipa.it) and Professor Ruggero De Maria, Institute of General Pathology, Università Cattolica del Sacro Cuore, Rome, Italy; [ruggero.demaria@unicatt.it](mailto:ruggero.demaria@unicatt.it)

LRM and AN contributed equally.

Received 8 November 2020

Revised 15 December 2020

Accepted 18 December 2020



© Author(s) (or their employer(s)) 2021. Re-use permitted under CC BY. Published by BMJ.

**To cite:** Mangiapane LR, Nicotra A, Turdo A, et al. *Gut* Epub ahead of print: [please include Day Month Year]. doi:10.1136/gutjnl-2020-323553

## ABSTRACT

**Objective** Cancer stem cells are responsible for tumour spreading and relapse. Human epidermal growth factor receptor 2 (HER2) expression is a negative prognostic factor in colorectal cancer (CRC) and a potential target in tumours carrying the gene amplification. Our aim was to define the expression of HER2 in colorectal cancer stem cells (CR-CSCs) and its possible role as therapeutic target in CRC resistant to anti-epidermal growth factor receptor (EGFR) therapy.

**Design** A collection of primary sphere cell cultures obtained from 60 CRC specimens was used to generate CR-CSC mouse avatars to preclinically validate therapeutic options. We also made use of the ChIP-seq analysis for transcriptional evaluation of HER2 activation and global RNA-seq to identify the mechanisms underlying therapy resistance.

**Results** Here we show that in CD44v6-positive CR-CSCs, high HER2 expression levels are associated with an activation of the phosphatidylinositol 3-kinase (PI3K)/AKT pathway, which promotes the acetylation at the regulatory elements of the *ErbB2* gene. HER2 targeting in combination with phosphatidylinositol 3-kinase (PI3K) and mitogen-activated protein kinase kinase (MEK) inhibitors induces CR-CSC death and regression of tumour xenografts, including those carrying *Kras* and *Pik3ca* mutation. Requirement for the triple targeting is due to the presence of cancer-associated fibroblasts, which release cytokines able to confer CR-CSC resistance to PI3K/AKT inhibitors. In contrast, targeting of PI3K/AKT as monotherapy is sufficient to kill liver-disseminating CR-CSCs in a model of adjuvant therapy.

**Conclusions** While PI3K targeting kills liver-colonising CR-CSCs, the concomitant inhibition of PI3K, HER2 and MEK is required to induce regression of tumours resistant to anti-EGFR therapies. These data may provide a rationale for designing clinical trials in the adjuvant and metastatic setting.

## INTRODUCTION

Despite major advances in terms of prevention and treatment, colorectal cancer (CRC) is one of the major causes of cancer-related death worldwide.<sup>1</sup> Diagnosis at stage IV and tumour progression after

surgery are very often lethal and require a substantial improvement of current therapeutic regimens. Over the past decade, the scientific community focused on different mechanisms found to be responsible for the development of therapy resistance, such as genetic heterogeneity and activation of alternative survival pathways.<sup>2</sup> Despite the availability of a large repertoire of new targeted therapeutics, there are not many options to treat patients with chemoresistant tumours, particularly if associated with activation of the signal pathway of rat sarcoma (RAS) or epidermal growth factor receptor (EGFR) resistance.

The expansion of resistant subclones due to tumour heterogeneity is now regarded as the major clinical hurdle in patient management.<sup>3</sup> About 36%–40% of patients with CRC are characterised by *Kras*-activating mutation at codons 12, 13 and 61, while 8%–15% present mutations in the *Braf* gene. In advanced stages, the presence of either *Braf* or *Ras* mutations correlates with a particularly poor prognosis.<sup>4</sup> Several studies have shown the predictive and prognostic roles of different gene mutations belonging to mitogen-activated protein kinase (MAPK) and phosphatidylinositol 3-kinase (PI3K)/AKT pathways, such as *Ras*, *Braf*, *Pik3ca* and *PTEN*.<sup>5,6</sup> EGFRs are the most important actionable targets identified so far in CRC. Although the addition of EGFR-targeting antibodies to chemotherapy is the most effective current therapy for *Ras* wild-type (wt) metastatic CRC, the therapeutic response is temporary and restricted to a limited number of patients due to primary or acquired resistance.<sup>7</sup> Repeated liquid biopsies accompanied by the analysis of tumour-associated genetic alterations would be needed to monitor the treatment responses and to adapt new targeted therapies.<sup>8</sup> The heterogeneity in the clinical responses of these patients with *Kras*-wt CRC has pointed out the contribution of other genetic mutations or amplifications.<sup>9</sup> For instance, beyond the *Ras* mutation, the activation of alternative or parallel downstream signalling inside or outside the MAPK pathways is involved in the anti-EGFR treatment inefficacy.<sup>7,10</sup> Thus, simultaneous inhibition of the EGFR family members and alternative signalling pathways has been adopted to

## Significance of this study

**What is already known on this subject?**

- ▶ Advanced colorectal cancer (CRC) remains essentially incurable, particularly in the presence of genomic alterations in the signalling pathway of rat sarcoma (RAS).
- ▶ Human epidermal growth factor receptor 2 (HER2) expression seems to correlate with the stage of disease and reduced survival in CRC.
- ▶ Targeting *ErbB2* amplification has a significant therapeutic activity in patients with CRC.
- ▶ The phosphatidylinositol 3-kinase (PI3K)/AKT pathway is constitutively activated in colorectal cancer stem cells (CR-CSCs) and sustains the expression of CD44v6, which drives the metastatic dissemination.

**What are the new findings?**

- ▶ The constitutive activation of PI3K/AKT is associated with high expression levels of HER2 in CD44v6-positive CR-CSCs.
- ▶ HER2, in combination with PI3K and mitogen-activated protein kinase kinase (MEK) inhibitors, leads to cancer stem cell death and tumour regression in CRC avatars resistant to anti-epidermal growth factor receptor (EGFR) therapy and to combinations of PI3K, BRAF and HER2 targeting.
- ▶ Liver disseminated CR-CSCs can be effectively killed by PI3K/AKT inhibitors in an experimental model of adjuvant therapy.
- ▶ Cytokines released by cancer-associated fibroblasts, particularly hepatocyte growth factor (HGF), stromal cell-derived factor-1 (SDF-1) and osteopontin (OPN), confer resistance to the targeting of the PI3K/AKT pathway and surrogate the protective effect of tumour microenvironment.

**How might it impact on clinical practice in the foreseeable future?**

- ▶ PI3K/AKT inhibitors could be effective in the adjuvant setting for CRC.
- ▶ Targeting HER2, MEK and PI3K may provide a valuable therapeutic strategy against anti-EGFR-resistant advanced CRCs.

overcome EGFR therapy resistance determined by the amplification of receptor tyrosine kinases.<sup>11 12</sup> In contrast to melanoma, CRCs harbouring *Braf* mutations are refractory to BRAF inhibitors, such as vemurafenib.<sup>13</sup> CRC resistance to BRAF inhibitors remains a major obstacle in clinical settings.<sup>14</sup> This unresponsiveness is sustained by the activation of a feedback loop involving EGFR and downstream pathways.<sup>15</sup> Although a recent phase II clinical study showed that addition of vemurafenib and cetuximab to chemotherapy prolonged the progression-free survival of metastatic patients with *Braf*-mutated tumours by 2.4 months, the prognosis of these patients remains poor.<sup>16</sup> Moreover, another recent study reported that the combined BRAF, EGFR and mitogen-activated protein kinase kinase (MEK) inhibition in patients with *Braf*<sup>V600E</sup>-mutant CRC could increase survival, even if patients experienced primary and acquired resistance due to a positive feedback regulation of MAPK pathway in tumour cells.<sup>17</sup>

Given that *Kras*-mutant CRCs display different resistance mechanisms to EGFR and MAPK inhibitors, many alternative strategies are currently under investigation.<sup>18</sup> In addition to acquired genetic mutations, the activation of a positive human epidermal growth factor receptor 2 (HER2) and HER3 feedback loop seems to be one example of antitumour therapy escape.<sup>19 20</sup> Accordingly, the combined treatment with MEK and

EGFR/HER2 dual inhibitors has shown a synergistic activity in preclinical models based on CRC cell lines bearing *Kras* mutation.<sup>21</sup> The investigation on EGFR family members in CRC has been recently focused on HER2. *ErbB2* amplification occurs in approximately 3%–10% of patients with CRC and may promote resistance to EGFR inhibitors.<sup>22 23</sup> Moreover, HER2 expression appears as a negative prognostic factor that correlates with the stage and survival in patients with CRC.<sup>24</sup> This hypothesis has been recently validated by the clinical trial Heracles, which showed that the combination of trastuzumab and lapatinib in *ErbB2*-amplified patients with CRC can induce the regression of tumours resistant to anti-EGFR therapies.<sup>25</sup> Constitutive expression of HER2 can be also driven by the degree of its enhancer and promoter activities.<sup>26</sup>

Myc overexpression may contribute to promote therapy resistance in *Kras*-mutant CRCs.<sup>27</sup> While the MAPK effector promotes Myc stabilisation, its proteosomal degradation is mediated by GSK3 $\beta$ .<sup>28 29</sup> The role of Myc in the tumorigenesis programme is mediated by the upregulation of the miR-17–92 cluster, which is associated with a poor prognosis.<sup>30</sup>

Colorectal cancer stem cells (CR-CSCs) are responsible for tumour development, spreading and resistance to chemotherapy.<sup>31 32</sup> We have created a large collection of primary CRC cells growing as spheroids and able to reproduce the patients' tumour in mouse avatars. We have recently shown that CR-CSCs express CD44v6 and depend on the PI3K/AKT pathway for survival and spreading.<sup>31 33</sup> Herein, we have studied the molecular pathways that should be targeted to kill CR-CSCs both in the adjuvant and metastatic settings. While targeting the PI3K/AKT pathway is sufficient to kill disseminating CR-CSCs, we found that HER2 is constitutively expressed in CR-CSCs and that the simultaneous targeting of HER2, PI3K and MEK neutralises the protective effect of tumour stroma and induces tumour regression, even in the presence of aggressive mutational backgrounds.

**METHODS**

A detailed description of the methods can be found in online supplemental information.

**RESULTS****CD44V6-positive CRC cells express high levels of HER2 and are cetuximab resistant**

EGFR inhibitors promote an effective therapeutic response in about 50%–55% of the patients with *Ras/Braf*-wt CRC, whereas *Braf*- and *Kras*-mutant CRC cells are completely resistant.<sup>9</sup> In accordance with clinical data, treatment with cetuximab affected the cell viability of about a half of the *Ras/Braf*-wt primary colorectal cancer sphere cells (CSphCs) and delayed the outgrowth of tumour xenografts (figure 1A, online supplemental figure 1A,B and online supplemental table 1).

Primary resistance to the EGFR blockade is mostly due to a constitutive activation of the RAS-MAPK signalling network.<sup>9</sup> Accordingly, a global RNA-Seq transcriptome analysis of cetuximab-resistant versus sensitive *Ras/Braf*-wt CSphCs showed 252 differentially expressed genes (DEGs) (online supplemental figure 1C and online supplemental table 2). The gene set enrichment analysis (GSEA) computed with the Molecular Signatures Database displayed the enrichment of genes associated with activation of the MAPK-signalling pathway, including the negative feedback regulator DUSP4<sup>34</sup> (figure 1B and online supplemental figure 1D). Besides the activation of signalling pathway of MAPK, *Ras/Braf*-wt CSphCs resistant to cetuximab showed higher mRNA expression levels of *ErbB2* compared with

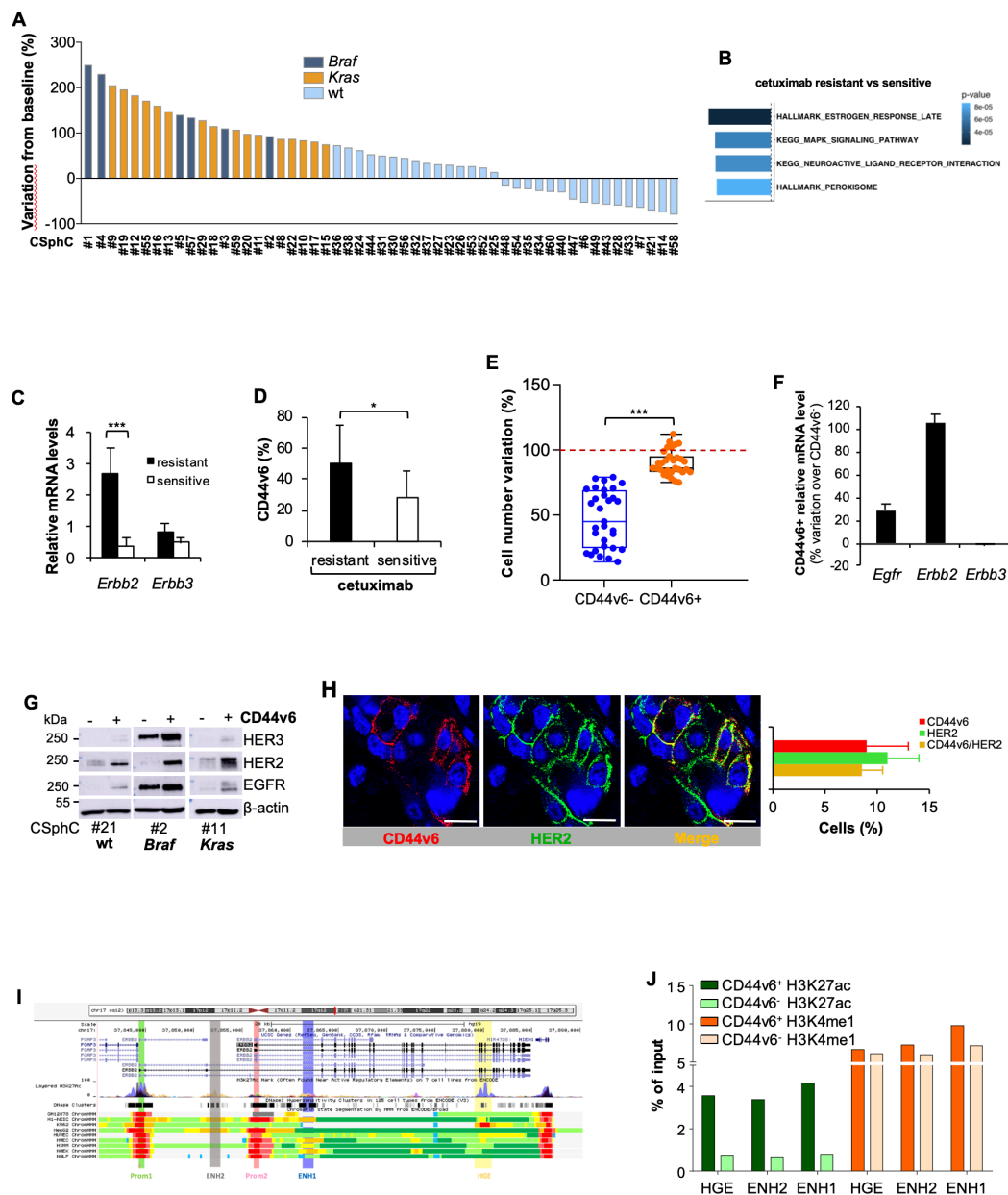


**Figure 1** High expression of HER2 confers resistance to anti-epidermal growth factor receptor (EGFR) treatment in CD44v6-positive CR-CSCs. (A) Waterfall plot of cetuximab response in *Ras/Braf*-wt, *Braf*-mutant and *Kras*-mutant CSphC lines following 72 hours of treatment. (B) Top four significantly enriched gene sets in hallmark, canonical pathways MSigDB collections (false discovery rate (FDR)  $Q$ -value  $\leq 0.05$ ) identified through the analysis of differentially expressed genes between cetuximab resistant versus sensitive *Ras/Braf*-wt sphere cells. P values related to each enriched gene set are indicated. (C) *ErbB2* and *ErbB3* mRNA expression levels in *Ras/Braf*-wt sphere cells resistant and sensitive to cetuximab. *Gapdh* amplification was used as endogenous control. Data are represented as  $\pm$ SD of three experiments performed with 31 *Ras/Braf*-wt. (D) CD44v6 expression performed in cells as in (C). (E) Viable cell number variation in enriched CD44v6<sup>-</sup> and CD44v6<sup>+</sup> CD44v6-positive *Ras/Braf*-wt treated with cetuximab for 72 hours and normalised with the values of cells treated with vehicle (indicated as 100%, red dotted line). Boxes and whiskers represent mean  $\pm$ SD of six experiments performed with 15 resistant and 16 sensitive *Ras/Braf*-wt sphere cells. (F) Variation of *Egfr*, *ErbB2* and *ErbB3* mRNA expression levels in CD44v6<sup>-</sup> versus CD44v6<sup>+</sup> cells. *Gapdh* amplification was used as endogenous control. Data are represented as mean  $\pm$ SD of nine experiments performed with three *Ras/Braf*-wt (CSphC#14, 21 and 33), three *Braf*-mutants (CSphC#1, 2 and 5) and three *Kras*-mutants (CSphC#10, 11 and 16). (G) Immunoblot analysis of HER3, HER2 and EGFR on purified CD44v6<sup>-</sup> and CD44v6<sup>+</sup> *Ras/Braf*-wt (CSphC#21), *Braf*-mutant (CSphC#2) and *Kras*-mutant (CSphC#11) CR-CSphC populations.  $\beta$ -Actin was used as loading control. (H, left panel) Representative immunofluorescence analysis of CD44v6 and HER2 on paraffin embedded sections from human CRC tissue specimen. Nuclei were counterstained with TOTO-3. Scale bars, 20  $\mu$ m. Percentages of CD44v6, HER2 and CD44v6/HER2 positivity in eight human CRC tissues are shown on the right panel. Data are mean  $\pm$ SD of eight different samples. (I) Browser view of the *ErbB2* locus, showing different isoforms of *ErbB2* and chromatin states (ChromHMM tracks). Two promoters and three potential enhancers are highlighted (Prom1, Prom2, ENH1, ENH2 and HGE). (J) ChIP-qPCR for the histone marks H3K27ac and H3K4me1 at the indicated enhancer regions (ENH1, ENH2 and HGE) in *Braf*-mutant cells positive or negative for CD44v6. Enrichment is indicated as % relative to the input. CR-CSC, colorectal cancer stem cell; CSphC, colorectal cancer sphere cell; ENH1, intron 1 enhancer; ENH2, intron 2 enhancer; HER2, human epidermal growth factor receptor 2; HGE, *HER2* gene body enhancer; MSigDB, Molecular Signatures Database; wt, wild type. \* indicates  $P < 0.05$  and \*\*\* indicates  $P < 0.001$ .



those sensitive (figure 1C). In line with literature,<sup>23</sup> our CSphC collection showed a 9.7% of *ErbB2* amplification (online supplemental table 1). We previously reported that while CD44v6 is a functional marker that identifies tumour-initiating CR-CSCs, the CD44v6-negative population represents the progenitor and differentiated fraction.<sup>31,33</sup> A cohort of 31 out of 47 primary CSphC lines showed that the high percentage of CD44v6 expression levels resided in the *Ras/Braf*-wt cells resistant to cetuximab, even though these expression levels are similarly distributed between *Ras/Braf*-wt, *Braf*-mutated and *Kras*-mutated cell lines (figure 1D and online supplemental figure 1E). Because the CD44v6-positive population, within the *Ras/Braf*-wt cells, is resistant and increases after treatment with cetuximab (figure 1E and online supplemental figure 1F), we investigated whether the expression in signalling pathways associated with drug resistance may differ between the stem and differentiated cell compartments. Reverse phosphoproteomic analysis (RPPA) of CSphCs showed that, while MAPK pathways and HER2 are highly regulated, EGFR and HER3 are expressed in a lesser extent in the CD44v6-positive than in the CD44v6<sup>-</sup> fraction (online supplemental figure 1G). The analysis at mRNA and protein levels confirmed an increased HER2 expression in the tumorigenic CD44v6-positive population of CRC cells, independently of the mutational background (figure 1F,G and online supplemental figure 1H,I). Accordingly, immunofluorescence analysis of patient tumour sections and tumour spheres indicated that the majority of CD44v6-positive cells coexpressed HER2 (figure 1H and online supplemental figure 1J).

We next investigated the transcriptional regulation of *ErbB2* expression in CD44v6-positive fraction by evaluating its 3' regulatory elements. Interestingly, H3K27 acetylation (H3K27ac) was enriched at the analysed regions of *HER2* gene body enhancer (HGE), intron 1 enhancer (ENH1) and intron 2 enhancer in CD44v6-positive compartment, whereas H3K4me1 enrichment was equally found in both CD44v6<sup>-</sup> and CD44v6-positive cell fractions at all three enhancer regions (figure 1I,J and online supplemental figure 1K). These data indicate that the enhancers are poised in both cellular fractions but only fully activated in the CD44v6-positive compartment, suggesting that the activation of *ErbB2* transcription mediated by the increased acetylation is restricted to the CD44v6-positive CRC cell compartment.

### PI3K/AKT pathway activation is associated with the transcriptional regulation of *ErbB2* in CD44v6-positive cells

The transcriptomic analysis of CD44v6<sup>high</sup> versus CD44v6<sup>low</sup> cells highlighted the presence of 173 DEGs (online supplemental figure 2A and online supplemental table 3). In CD44v6<sup>high</sup> cells, the GSEA enriched for genes related to the activation of PI3K/AKT signalling pathway, such as NOS3<sup>35</sup> (figure 2A and online supplemental figure 2B). To investigate the role of PI3K in the transcriptional regulation of *ErbB2*, we induced an activating *Pik3ca* mutation into *Pik3ca*-wt low expressing HER2 CSphC lines by using CRISPR nuclease in combination with a specific donor DNA that introduced the *E545K* point mutation (online supplemental figure 2C and online supplemental table 1). The presence of a *Pik3ca*<sup>E545K</sup> is associated with an increased expression of HER2 and phospho-AKT (figure 2B,C and online supplemental figure 2D). Interestingly, immunofluorescence analysis of primary tumour sections indicated that HER2-positive cells were mainly prominent in the tumour invasion front and displayed activation of the PI3K/AKT pathway (figure 2D). The essential role of PI3K in the transcriptional regulation of *ErbB2* was further supported by CHIP-qPCR analysis showing that overexpression

of the mostly represented *Pik3ca* activating mutation in breast cancer, the *Pik3ca*<sup>H1047R</sup>, in mammary IMEC-MYC cells enhances the transcriptional activity of both *ErbB2* promoters (prom 1 and prom 2) and ENH1 and HGE (online supplemental figure 2E). Since the inhibition of the PI3K/AKT pathway hampers the cell viability of CD44v6-positive cells,<sup>33</sup> we evaluated whether the addition of a PI3K inhibitor to the combination therapy could affect the viability of both CD44v6-positive and CD44v6<sup>-</sup> cells. To confirm the dependence of CR-CSCs on the PI3K activity, we tested an AKT (miransertib) and two PI3K (BKM120 and taselisib) inhibitors on several primary CSphC lines. Both miransertib and PI3K inhibitors reduced considerably the viability of CD44v6-positive cells in vitro regardless of the mutational background (online supplemental figure 2F–H), confirming that the PI3K/AKT pathway plays a key role on CR-CSC survival.

We previously showed that CRC development is sustained by cancer stem cells (CSCs), whose dissemination is responsible for CRC metastasis,<sup>33</sup> suggesting that targeting disseminated CR-CSCs may prevent tumour relapse and increase survival of patients with CRC.<sup>31</sup> Thus, we investigated the ability of PI3K inhibitors to target disseminated sphere cells in the liver before they were able to make metastases in a model of adjuvant treatment. We found that the administration of taselisib in immunocompromised mice was able to prevent the formation of liver metastases after dissemination of CSphCs by spleen injection (figure 2E). These findings support the investigation of PI3K/AKT inhibitors in clinical trials aiming at killing disseminated metastasis-initiating CR-CSCs. The different survival properties of CD44v6 cells in vitro and in established tumours are likely due to the protective activity of the tumour microenvironment.<sup>31</sup> Outside the protective tumour context, PI3K and AKT inhibitors can kill CR-CSCs. In contrast, the protective activity of cells and cytokines present in the tumour microenvironment may require the targeting of multiple pathways to overcome the enhanced survival of CR-CSCs. This hypothesis is supported by the significant therapeutic activity of PI3K inhibitors on micrometastases and small tumour lesions.<sup>36</sup> In order to identify some possible soluble mediators of such protective activity, we then measured the release of cytokines from cancer-associated fibroblasts (CAFs). Among the cytokines more abundantly produced by CAFs, we selected HGF, SDF-1 and OPN (figure 2F) to further investigation, based on their ability to support PI3K/AKT activity and stemness properties in CSphCs.<sup>33</sup> We next investigated whether the presence of CAFs would influence the survival of CSphCs exposed to the PI3K inhibitor. The coculture of GFP-labelled tumour spheres with CAFs protected cells from taselisib treatment (figure 2G), suggesting that CAFs could play a critical role in opposition to the killing activity of PI3K inhibitors in CRC. Moreover, neutralisation of HGF, SDF-1 and OPN completely prevented the protective activity of CAFs (figure 2H), indicating that these cytokines are responsible for delivering a survival signal in CR-CSCs that makes ineffective the PI3K targeting. Exposure of CSphCs, CD44v6-positive and CD44v6<sup>-</sup> cell fractions to CAF-released cytokines enhanced the expression of *ErbB2* mRNA (figure 2I and online supplemental figure 2I). Interestingly, in the presence of tumour microenvironmental cytokines, *ErbB2* expression levels were not affected by the treatment with the PI3K inhibitor (online supplemental figure 2J–L). We also observed that HGF plays a major role in CAF-mediated protection of CSphCs treated with taselisib (figure 2J). Taken together, these data suggest that the tumour microenvironment protects CR-CSCs from the targeting of the PI3K/AKT pathway.



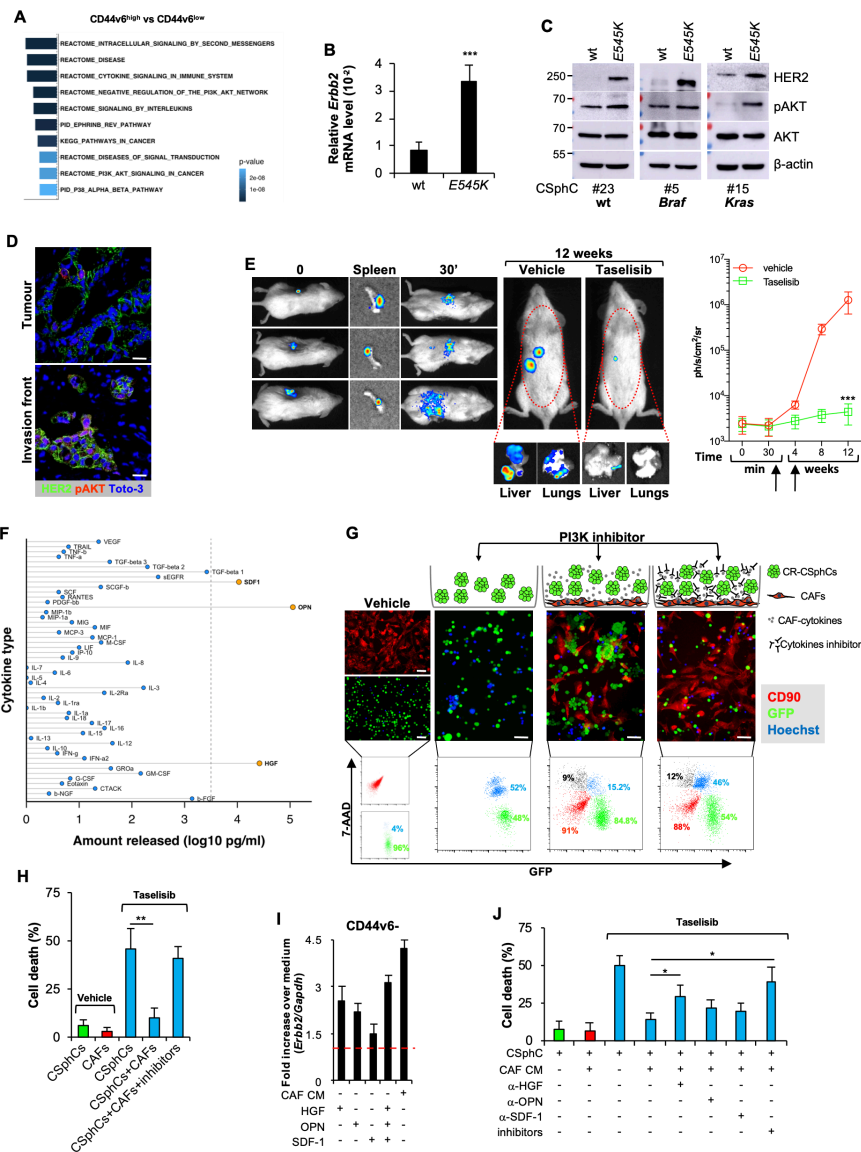


**Figure 2** Activation of PI3K/AKT pathway is accompanied by elevated *ErbB2* expression levels in CD44v6-positive CRC cells. (A) Top 10 significantly enriched gene sets in hallmark, canonical pathways MSigDB collections (FDR Q-value $\leq$ 0.05) computed by the analysis of differentially expressed genes between CD44v6<sup>high</sup> and CD44v6<sup>low</sup> cells. (B) mRNA relative levels of *ErbB2* in CSphCs and their corresponding CRISPR/Cas9-*Pik3ca*<sup>E545K</sup> cells. Data are represented as mean $\pm$ SD of six independent experiments performed with *Ras/Braf*-wt (CSphC#23), *Braf*-mutant (CSphC#5) and *Kras*-mutant (CSphC#15) cells and their corresponding CRISPR/Cas9-*Pik3ca*<sup>E545K</sup> cells. (C) Immunoblot analysis of HER2, pAKT and AKT on *Ras/Braf*-wt (CSphC#23), *Braf*-mutant (CSphC#5) *Kras*-mutant (CSphC#15) cells.  $\beta$ -Actin was used as loading control. (D) Representative immunofluorescence analysis of HER2 and pAKT on paraffin-embedded sections from six human CRC tissue specimens. Nuclei were counterstained with TOTO-3. Scale bars, 20  $\mu$ m. (E, left panels) In vivo whole-body imaging analysis of mice at 0 and 30 min and 12 weeks injected with sphere cells into the spleen. Five days after cell injection, mice were treated daily with taselisib for 3 weeks. Signal within the red dotted area represents the bioluminescence quantification. Kinetics of metastasis formation at the indicated time points (right panels). Black arrows indicate the start and end of treatment (from day 6 to week 4). Data are mean $\pm$ SD of four independent experiments of six mice per group using *Kras*-mutant (CSphC#8 and 11) sphere cell lines. (F) Lollipop plot representing the amount of cytokines released by immortalised CAFs. Data are mean of six independent experiments using cells purified from six different patients. (G) Cell death (blue colour) evaluated by immunofluorescence (upper panels) and flow cytometry (lower panels) in sphere cells (CSphC#8) transduced with GFP (green colour) cocultured with CAFs CD90 positive (red colour) and treated with a PI3K inhibitor (taselisib) for 72 hours in the presence or absence of hepatocyte growth factor (HGF), stromal cell-derived factor-1 (SDF-1) and osteopontin (OPN) blocking antibodies (inhibitors). Scale bars, 40  $\mu$ m. (H) Percentage of cell death in cells as in (G). Data are mean $\pm$ SD of three independent experiments using *Ras/Braf*-wt (CSphC#14, 21 and 33), *Braf*-mutant (CSphC#1, 2 and 5) and *Kras*-mutant (CSphC#8, 10 and 11) sphere cell lines. (I) *ErbB2* mRNA expression levels in CD44v6<sup>-</sup> enriched cells treated with CAF CM and the indicated cytokines. Data are mean $\pm$ SD of three independent experiments performed with cells derived from *Ras/Braf*-wt (CSphC#14 and 33), *Braf*-mutant (CSphC#1 and 5) and *Kras*-mutant (CSphC#10 and 11) sphere cell lines. (J) Cell death in sphere cells exposed to CAF CM and treated with taselisib for 72 hours in the presence of cytokine neutralising antibodies as indicated. Data are mean $\pm$ SD of three independent experiments performed with *Ras/Braf*-wt (CSphC#6, 14, 21 and 33), *Braf*-mutant (CSphC#1, 2, 4 and 5) and *Kras*-mutant (CSphC#8, 10, 11 and 17) sphere cell lines. CAF, cancer-associated fibroblast; CM, conditioned medium; CRC, colorectal cancer; CSphC, colorectal cancer sphere cell; HER2, human epidermal growth factor receptor 2; MSigDB, Molecular Signatures Database; wt, wild type. \*indicates P<0.05, \*\* indicates P<0.01 and \*\*\* indicates P<0.001.

## MEK sustains CR-CSCs resistance to the triple targeting of HER2, BRAF and PI3K

To further analyse the therapeutic potential of PI3K inhibitor in combination with MAPK pathway targeting, tumour xenografts, generated by the subcutaneous injection of CSphCs, were initially treated with either trastuzumab or cetuximab in combination with BRAF and PI3K inhibitors. These treatments were largely ineffective. We observed only a transient stabilisation of *Braf*-mutated tumours and a short delay in the disease progression of *Ras/Braf*-wt and *Kras*-mutated tumours (figure 3A and online supplemental figure 3A). These experiments allowed us to evaluate the potential mechanisms of acquired resistance to such triple combinations. CSphCs surviving the combinatorial treatment showed a significant phosphorylation of p235–236 S6 kinase (online supplemental figure 3B), which could follow the activation of RAS/ERK and mammalian target of rapamycin (mTOR) and result in the engagement of the Myc pathway.<sup>37,38</sup> The activation of PI3K/AKT and MAPK pathways were confirmed by western blot in tumour specimen-derived subcutaneous xenograft treated with the triple combination (figure 3B and online supplemental figure 3C). This phenomenon was paralleled by a strong activation of the PI3K/AKT and MAPK pathways, particularly in the presence of *Braf* or *Kras* mutations (figure 3B). Moreover, cells surviving the combinatorial treatment showed high expression levels of the miR-17–92 cluster (online supplemental figure 3D), whose upregulation is associated with Myc expression.<sup>39</sup> Altogether, these findings indicate that PI3K and MEK promote CR-CSC resistance to the targeting of BRAF, HER2 and PI3K signalling pathways.

Replacement of BRAF targeting with a MEK inhibitor caused a marked reduction of the PI3K/AKT and MAPK pathway activation and a decrease of phosphorylation of S6 kinase (figure 3C and online supplemental figure 3E,F). Viability of CSphCs was severely affected by the use of trametinib combination regardless of the mutational status and remarkably diminished the Myc-regulated miRNAs in cells previously exposed to vemurafenib-based combination (online supplemental figure 3G,H).

We then investigated whether the MEK inhibitor-based combination is also able to overcome the protective effect mediated by the tumour microenvironment. Beside PI3K, CAF-released cytokines boosted MAPK pathway activation, which persisted after the treatment of CSphCs with vemurafenib-based combination therapy (figure 3D). Conversely, pharmacological targeting of MEK, instead of BRAF, promoted a considerable cell death, paralleled with a marked reduction of MEK/ERK, AKT activation and Myc expression in CSphCs, independently of the presence of *ErbB2* amplification and the exposure to CAF conditioned medium (figure 3D,E and online supplemental figure 3I). Of note, sphere cells able to survive to a prolonged exposure to the vemurafenib-based treatment remain sensitive to the triplet containing trametinib (online supplemental figure 3J). Altogether, these data suggest that the tumour microenvironment confers therapy resistance mediated by Myc through the activation of MAPK and PI3K–AKT pathways.

## MEK inhibition-based therapy is synthetically lethal in CR-CSCs

In line with these results, we found that the replacement of vemurafenib with MEK inhibitors in the triple combination prevented the tumorigenic activity retained by sphere cells (figure 4A,B) and tumour progression when delivered in vivo, as indicated by the decrease in Ki67, CD44v6 and CK20 expression (figure 4C,D and online supplemental figure 4A–C). Of note,

*Braf*-mutated or *Kras*-mutated xenograft tumours that recurred following the treatment with the vemurafenib-based triple combination, tumor xenografts resulted very sensitive to the trametinib-based combination therapy, as shown by the massive tumour regression and lack of regrowth even 6 weeks after treatment suspension (figure 4E). Next, we examined whether this MEK-targeted triplet was effective on a large number of primary CSphC cultures of different mutational backgrounds and their corresponding tumour xenografts. To confirm the effectiveness of this treatment, we tested other MEK and PI3K inhibitors (cobimetinib and taselisib) in combination with trastuzumab. Importantly, tumour size generated by the subcutaneous injection of primary sphere cells was significantly hampered by the treatment with either trametinib in combination with trastuzumab and BKM120 or cobimetinib plus trastuzumab and taselisib, independently of the mutational status (figure 4A and online supplemental figure 4D,E). Of note, this latter combination remarkably reduced the CD44v6 expression level on xenograft-derived CRC cells (online supplemental figure 4F). Consistently, cobimetinib plus trastuzumab and taselisib induced the death of a conspicuous number of cells that were substituted by fibrosis, resulting in a considerable decrease in the amount of Ki67-positive and CK20-positive cells (online supplemental figure 4G). Thus, simultaneous MEK/HER2/PI3K inhibition exerted a potent anti-tumour activity in CRC xenografts regardless of the mutational status. Altogether these data demonstrate that the combination treatment with HER2, PI3K and MEK inhibitors is synthetically lethal for CRC cells (figure 4F).

## DISCUSSION

The currently available targeted therapies for advanced CRC have a limited effect, particularly on the survival of patients carrying tumours with *Kras* mutation.<sup>5</sup> We recently demonstrated that CD44v6-positive CR-CSCs are responsible for metastatic spreading and have a constitutive activation of the PI3K/AKT pathway that appears essential for their survival.<sup>33</sup> Here, we demonstrate that CR-CSCs express high levels of HER2, which are associated with a constitutive activation of the PI3K/AKT pathway. Inhibition of HER2, MEK and PI3K kills CR-CSCs and promotes a long-lasting regression of all the tumour xenografts tested, regardless of their mutational background.

Among the attempts to target the actionable mutations in CRC, the treatment with anti-HER2 in patients carrying *ErbB2* amplification has been successful in clinical trials, whereas patients with *Braf*<sup>V600E</sup>-mutant CRC are poorly responsive to the administration of vemurafenib or dabrafenib.<sup>13,40</sup>

Although the existence of synthetic lethality between BRAF and EGFR in *Braf*-mutated CRC cells would predict the potential therapeutic effect of a combined targeting, we found that CR-CSCs are resistant to the combination of anti-EGFR or anti-HER2 and BRAF inhibitors due to the constitutive activation of the PI3K/AKT pathway. This could be the reason why vemurafenib, in combination with irinotecan and cetuximab, showed a weak therapeutic effect in patients with metastatic CRC.<sup>41</sup>

Here, we found that the regulatory elements of *ErbB2* transcription are acetylated in CD44v6-positive cells. While this can explain why CR-CSCs are remarked by high HER2 expression, the potential ability of PI3K to promote a transcriptional activation of *ErbB2* corroborates the hypothesis that both of these oncogenic pathways should be targeted simultaneously. Since HER2 expression is lost on CR-CSC differentiation, it is likely that the specific expression of HER2 in the CD44v6-positive

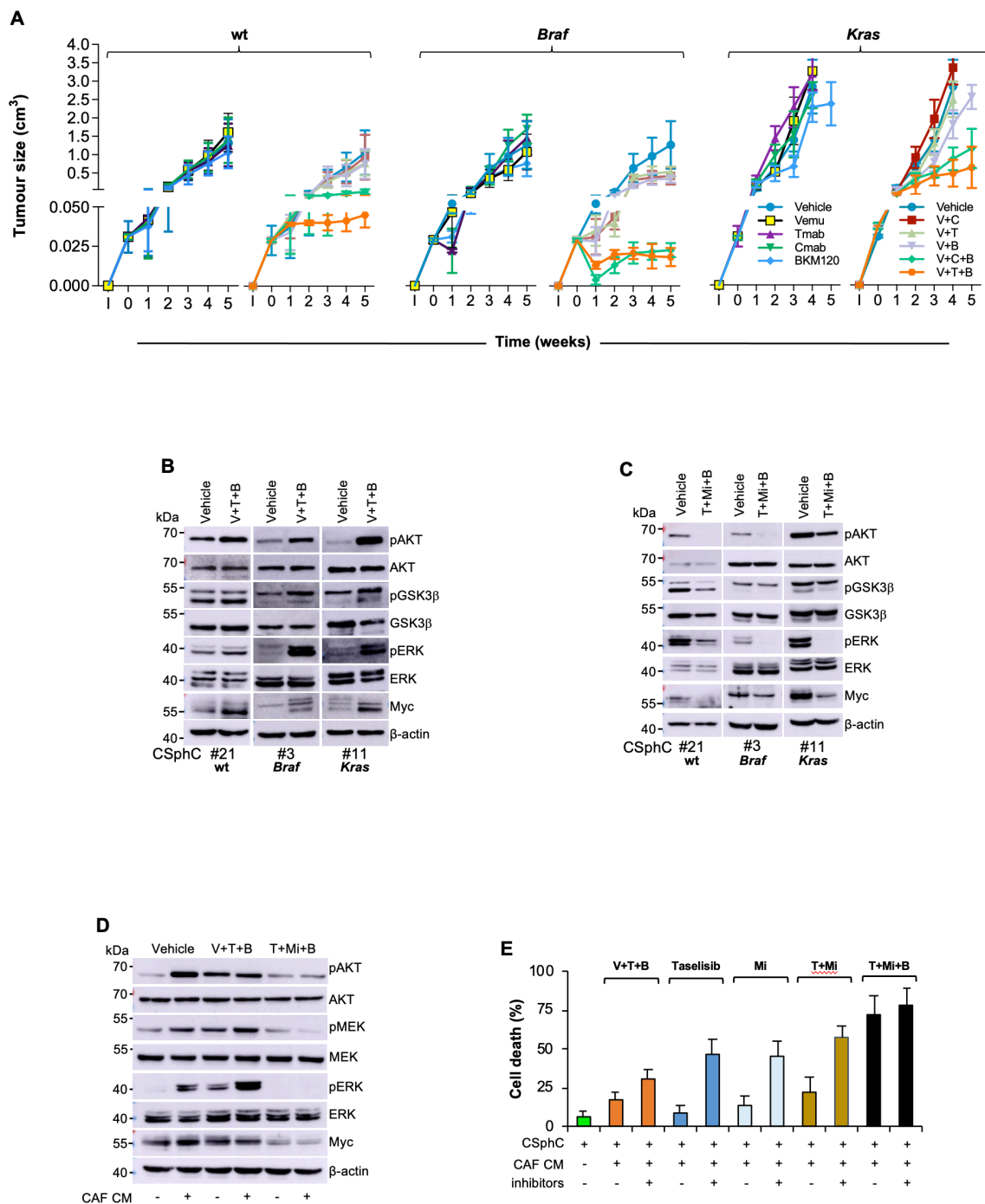


**Figure 3** HER2/MEK/PI3K combinatorial targeting counteracts the protective effect of cytokines produced by CAF. (A) Size of xenograft tumours generated by subcutaneous injection of *Ras/Braf*-wt (CSphC#14, 21 and 33), *Braf*-mutant (CSphC#1, 2, 3 and 5) or *Kras*-mutant (CSphC#8, 11 and 16) sphere cells. Mice were treated for the first 4 weeks with vehicle (vehicle) or Vemu (or V), cetuximab (Cmab or C), Tmab (or T) and a PI3K inhibitor (B) alone or in combination as indicated. 'I' indicates the time of cell injection. Treatment was started at time 0. Data are mean values of six independent experiments ( $n=6$  mice per group). (B) Immunoblot analysis of pAKT, AKT, pGSK3 $\beta$ , GSK3 $\beta$ , pERK, ERK and Myc on tumour xenograft-derived cells of mice injected with *Ras/Braf/Braf*-wt (CSphC#21), *Braf*-mutant (CSphC#3), *Kras*-mutant (CSphC#11) sphere cells. Mice were treated with vehicle or V in combination with T and B, and sacrificed 1 week after the treatment suspension (5 weeks).  $\beta$ -Actin was used as loading control. (C) Representative Western blot analysis of pAKT, AKT, pGSK3 $\beta$ , GSK3 $\beta$ , pERK, ERK and Myc in *Ras/Braf*-wt (CSphC#21), *Braf*-mutant (CSphC#3), *Kras*-mutant (CSphC#11) sphere cells treated for 24 hours with vehicle or T+Mi+B.  $\beta$ -Actin was used as loading control. (D) Immunoblot analysis of the indicated proteins in *Kras*-mutant (CSphC#9) sphere cells treated with vehicle or V in combination with T and B or T+Mi+B cultured in fetal bovine serum (FBS)-free Dulbecco's modified eagle medium (DMEM) or CAF CM for 24 hours. (E) Cell death percentage in CSphCs exposed to hepatocyte growth factor (HGF), stromal cell-derived factor-1 (SDF-1) and osteopontin (OPN) blocking antibodies (inhibitors) and treated as indicated for 72 hours. Data are mean $\pm$ SD of three independent experiments performed with *Ras/Braf*-wt (CSphC#14, 21 and 33), *Braf*-mutant (CSphC#1, 2 and 5) and *Kras*-mutant (CSphC#8, 10 and 11) sphere cell lines. B, BKM120; CAF, cancer-associated fibroblast; CSphC, colorectal cancer sphere cell; T, trastuzumab; T+Mi+B, trastuzumab in combination with MEKi and BKM120; V, vemurafenib; V+T+B, vemurafenib in combination with trastuzumab and BKM120; wt, wild type; CM, conditioned medium.



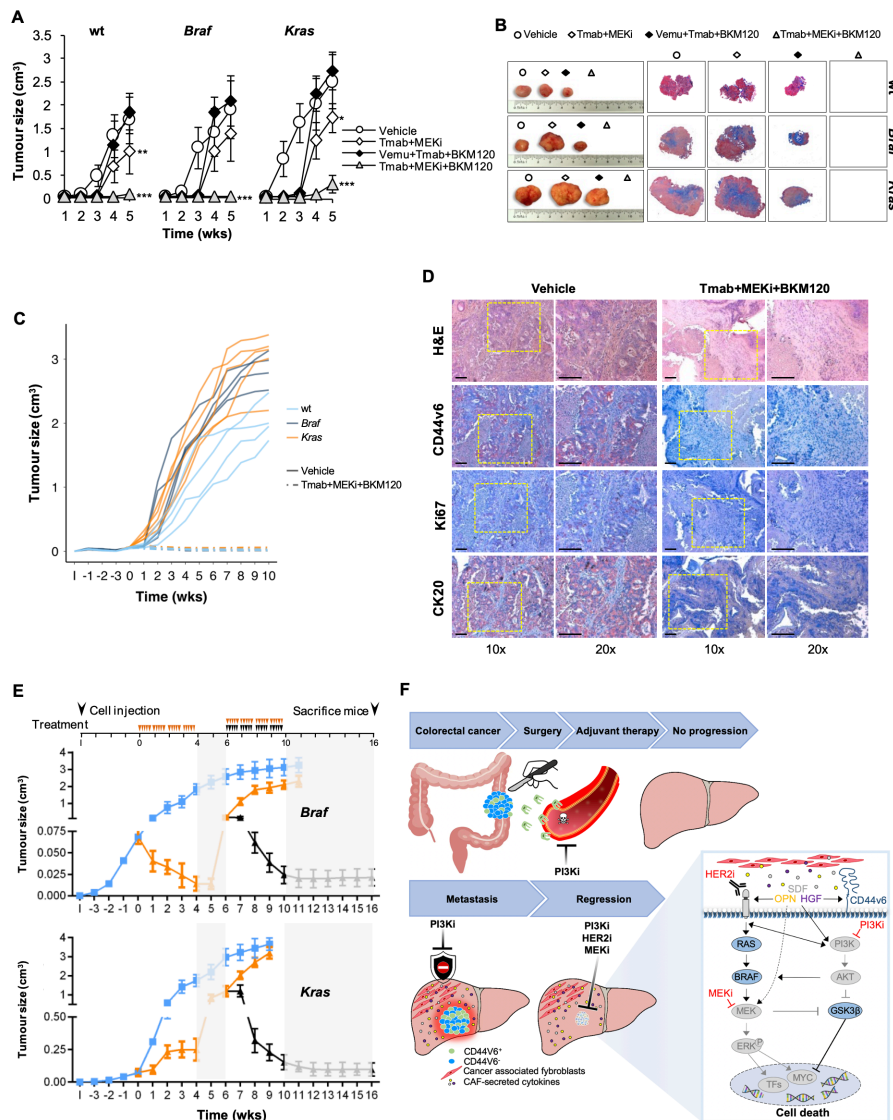


**Figure 4** Therapeutic potential of HER2, PI3K and MEK targeting in CRC. (A) Size of tumours generated by subcutaneous injection of surviving *Ras/Braf*-wt (CSphC#14, 21 and 33), *Braf*-mutant (CSphC#1, 2 and 5) and *Kras*-mutant (CSphC#8, 11 and 16) sphere cells after 5 days of in vitro combination treatment as indicated. Data reported are mean $\pm$ SD of tumour size for each cell lines ( $n=6$  mice per group). (B) Representative macroscopic and Azan-Mallory analysis on tumour xenografts at 5 weeks treated as in (A). (C) Individual subcutaneous tumour volume plots of mice generated by the injection of four CSphC lines bearing the indicated different mutational background and treated for 4 weeks (0–4 weeks) with vehicle (vehicle) or Tmab plus MEKi plus BKM120. 'I' indicates the time of cell injection. Treatment was started at time 0. Data show kinetic growth of xenograft tumours generated by the injection of *Ras/Braf*-wt (CSphC#14, 21, 33 and 56), *Braf*-mutant (CSphC#1, 2, 3 and 5) and *Kras*-mutant (CSphC#8, 9, 11 and 16) CSphCs. (D) Representative H&E and immunohistochemical analysis of CD44v6, Ki67 and CK20 on tumour xenografts generated by the injection of *Kras*-mutant (CSphC#11) sphere cells treated as in (C) at the time of sacrifice (10 weeks). Scale bars, 200  $\mu$ m. (E) Tumour size of mice xenografted with *Braf*-mutant (CSphC#1–5) and *Kras*-mutant (CSphC#8, 9, 11, 13 and 16) mutant sphere cells. Mice were treated with vehicle (vehicle, blue lines) or sequential treatments. A combination of Vemu, Tmab, BKM120 (Vemu+Tmab+BKM120, orange line) was used as first line (0–4 weeks, orange arrowheads) and after 2 weeks off-treatments, Tmab in combination with MEKi and BKM120 (Tmab+MEKi+BKM120, black lines and arrowheads) or the same Vemu combination used in the first 4 weeks (orange arrowheads) was administered from weeks 6 to 10. Off-treatments are highlighted with grey regions. 'I' indicates the time of cell injection. Data are expressed as mean $\pm$ SD of subcutaneously implanted CSphC lines for each mutational status ( $n=6$  mice per group). (F) Scheme of the signalling axis illustrating the site of action of the triple combination therapy. Surgery is the main treatment for primary CRC followed by adjuvant therapy. PI3Ki has shown efficacy in targeting disseminating CRC cells, impeding tumour progression (upper panel). However, PI3Ki as single agents are unable to counteract the TME protective influence in metastatic lesions. Triple combination treatment (PI3Ki, HER2i and MEKi) induces tumour regression by overcoming CAF-secreted cytokine effect (lower left panel). In CD44v6-positive CR-CSCs characterised by high PI3K pathway activity, TME-derived cytokines upregulate HER2 and CD44v6 expression levels, activate mitogen-activated protein kinase (MAPK) pathway and increase Myc protein levels, jeopardising the potential therapeutic efficacy of PI3Ki. The additional targeting of HER2 and the Myc upstream kinase MEK achieves a synthetic lethal effect in CR-CSCs (lower right panel). HER2, BRAF, PI3K and MEK inhibitors are indicated as I. CAF, cancer-associated fibroblast; CRC, colorectal cancer; CR-CSC, colorectal cancer cancer stem cell; CSphC, colorectal cancer sphere cell; HER2, human epidermal growth factor receptor 2; MEKi, trametinib; PI3Ki, PI3K inhibitors; TF, transcriptional factor; Tmab, trastuzumab; TME, tumour microenvironment; Vemu, vemurafenib; wt, wild type. \* indicates  $P<0.05$ , \*\* indicates  $P<0.01$  and \*\*\* indicates  $P<0.001$ .

cell compartment results from the considerable reduction of the PI3K/AKT signalling pathway and  $\beta$ -catenin activity observed in their differentiated progeny.<sup>33</sup>

Although sphere culture models mostly recapitulate the genetic landscape and the transcriptomic profile of parental tumour, representing valuable preliminary tools to identify potentially effective targeted therapies,<sup>42–43</sup> it is fundamental to dissect the tumour microenvironment contribution in mediating resistance of cancer cells to therapeutic drugs.

According to our previous observation, we found that tumour microenvironmental cytokines produced by CAFs contribute to recapitulate a protective effect against antitumour drugs expanding the CD44v6-positive compartment expressing HER2. We showed that HGF and to a lesser extent OPN and SDF-1 make CR-CSCs resistant to the targeting of the PI3K/AKT pathway, possibly explaining the disappointing results obtained in the clinical trials that evaluated the therapeutic effects of PI3K inhibitors in metastatic patients.<sup>44</sup> Such vulnerability of CR-CSCs in the absence of CAFs suggests that PI3K/AKT inhibitors can contribute to kill cells disseminated into the liver as part of adjuvant treatment due to the absence of a protective microenvironment. This hypothesis is strengthened by the observation that treatment with tasislisib prevents the formation of liver metastases in mice receiving sphere cells by spleen injection.

In a subsequent set of experiments, we show that the addition of PI3K inhibitors to the combination of vemurafenib with trastuzumab or cetuximab induces a partial response of *Braf*-mutated tumours and a temporary stabilisation followed by a slower progression of *Ras/Braf*-wt and *Kras*-mutated tumours. Such transient therapeutic effect induces the rapid accumulation of tumour-initiating cells resistant to this triplet likely due to the presence of tumour microenvironmental cytokines.

The RPPA analysis in residual CSphCs spared by the HER2/BRAF/PI3K targeting allowed us to identify, through the regulation of S6 kinase phosphorylation, MEK and PI3K as major components of the resistance pathway. Accordingly, we observed increased levels of Myc in cells simultaneously exposed to agents targeting HER2, BRAF and PI3K. The concomitant activation of S6 kinase and MEK in sphere cells resistant to the vemurafenib-based triple combinations suggests that the failure to target both RAF and PI3K downstream pathways is responsible for maintaining activation of ERK and high Myc levels and promoting the pharmacological resistance of CR-CSCs to this triplet.

MEK is a key downstream element of the RAS-RAF pathway able to indirectly activate Myc.<sup>15</sup> Replacement of vemurafenib with MEK inhibitors in the triple combination was able to significantly limit ERK activation and downregulate Myc expression while inducing a considerable therapeutic response in *Braf*-mutated and *Kras*-mutated tumours progressing after the vemurafenib-based combination. Of note, our data showed that MEK inhibition-based triplets were able to kill CR-CSCs in the presence of cytokines released by CAFs and to induce tumour regression in all CR-CSC-based xenografts tested, regardless of the mutational status and *ErbB2* amplification. Hence, HER2, PI3K and MEK appear as critical therapeutic targets in CR-CSCs, independently of the genomic abnormalities developed in patients' tumours. This combination appears the most active both in tumour xenografts and in the in vitro experiments designed in the presence of the CAF-released cytokines.

The advent of targeted therapies and the study of the associated resistance mechanisms revealed the presence of clonal heterogeneity in CRC.<sup>45</sup> Most of the current therapeutic strategies, including targeted combination treatments, affect differentiated cells and spare CSCs that eventually reinitiate tumour growth. It

is therefore clear that the identification of the critical pathways responsible for the increase of survival and therapy resistance of CR-CSCs appears as a major priority to define possible effective treatments for patients with advanced CRC. This is particularly true for metastatic patients carrying oncogenic alterations in the RAS pathway, who have very limited therapeutic options. Our data show that MEK inhibition in association with PI3K and HER2 targeting can induce tumour regression even in tumours carrying mutations in the RAS pathway. Although targeted therapy is less toxic than standard chemotherapy, EGFR inhibitors are commonly associated with adverse events, including the inhibition of the MEK/ERK signal pathway, which compromises the epidermis cell differentiation leading to skin lesions.<sup>46</sup> Given that HER2 inhibitors generally display minimal dermatological side effects as compared with those induced by EGFR inhibitors,<sup>23</sup> as shown by current clinical studies for the treatment of advanced CRC,<sup>25</sup> we foresee that triple targeting of HER2, MEK and PI3K may have a superior patient compliance and overall treatment outcome.

Here, we have shown that some biological features of CR-CSCs have the potential to be exploited in the clinics. The specific expression of HER2 in CR-CSCs, independently of gene amplification, suggests that HER2 should be regarded as key therapeutic target that deserves further preclinical and clinical investigations in CRC. The good therapeutic response, observed in clinical trial by HER2 targeting in patients with amplified tumours, increases the feasibility of this approach. Moreover, we provide evidence that targeting of the PI3K/AKT pathway could be exploited both in advanced disease and in the adjuvant setting. These findings may help define new therapeutic strategies based on CR-CSC targeting.

#### Author affiliations

<sup>1</sup>Department of Surgical, Oncological and Stomatological Sciences, Università degli Studi di Palermo, Palermo, Italy

<sup>2</sup>Department of Health Promotion Sciences, Internal Medicine and Medical Specialties, Università degli Studi di Palermo, Palermo, Italy

<sup>3</sup>Core Facilities, Istituto Superiore di Sanità, Roma, Italy

<sup>4</sup>Department of Cellular, Computational, and Integrative Biology (CIBIO), University of Trento, Trento, Italy

<sup>5</sup>Department of Oncology and Molecular Medicine, Istituto Superiore di Sanità, Roma, Italy

<sup>6</sup>Laboratory for Experimental Oncology and Radiobiology, Center for Experimental and Molecular Medicine, University of Amsterdam, Amsterdam, Noord-Holland, The Netherlands

<sup>7</sup>Onco Institute, University of Amsterdam, Amsterdam, Noord-Holland, The Netherlands

<sup>8</sup>Institute of General Pathology, Università Cattolica del Sacro Cuore Facoltà di Medicina e Chirurgia, Roma, Italy

<sup>9</sup>Policlinico A Gemelli, Roma, Lazio, Italy

**Acknowledgements** We thank Francesco Calò for graphic image editing and Alice Alferi for technical assistance. LRM is a student of the Molecular and Clinical Medicine PhD Program. AT and VV are research fellows funded by European Union-FESR FSE, PON Ricerca e Innovazione 2014–2020 (AIM line 1).

**Contributors** LRM, AN, RDM and GS conceived and designed the project. Experiments were conducted by LRM, AN, AT, MG, PB, SDF, VV, MS, SB, LF, MEF, MLI, IP, GGA and MT. Data provision and bioinformatic analysis were carried out by DSS, MS, SB, JPM and AZ. Pathology support, tissue provision and intellectual input were from MEF, MRB and GGu. RDM and GS wrote the manuscript.

**Funding** This work was supported by AIRC 5x1000 (9979) to GS and RDM, AIRC IG (22911) to AZ and AIRC IG (21445) and PRIN (2017WKNLSL) to GS.

**Competing interests** None declared.

**Patient consent for publication** Not required.

**Provenance and peer review** Not commissioned; externally peer reviewed.

**Data availability statement** Data are available in a public, open access repository. All data relevant to the study are included in the article or uploaded as supplementary information. The data that support the findings of this study

are available from the corresponding author (GS) upon reasonable request. RNA sequencing data of CR-CSPhCs have been deposited in a public, open access GEO repository, under accession number GSE162104 (link to data: <https://www.ncbi.nlm.nih.gov/geo/query/acc.cgi?acc=GSE162104>).

**Supplemental material** This content has been supplied by the author(s). It has not been vetted by BMJ Publishing Group Limited (BMJ) and may not have been peer-reviewed. Any opinions or recommendations discussed are solely those of the author(s) and are not endorsed by BMJ. BMJ disclaims all liability and responsibility arising from any reliance placed on the content. Where the content includes any translated material, BMJ does not warrant the accuracy and reliability of the translations (including but not limited to local regulations, clinical guidelines, terminology, drug names and drug dosages), and is not responsible for any error and/or omissions arising from translation and adaptation or otherwise.

**Open access** This is an open access article distributed in accordance with the Creative Commons Attribution 4.0 Unported (CC BY 4.0) license, which permits others to copy, redistribute, remix, transform and build upon this work for any purpose, provided the original work is properly cited, a link to the licence is given, and indication of whether changes were made. See: <https://creativecommons.org/licenses/by/4.0/>.

#### ORCID iDs

Alice Turdo <http://orcid.org/0000-0002-6152-4903>  
 Michele Signore <http://orcid.org/0000-0002-0262-842X>  
 Luca Fagnocchi <http://orcid.org/0000-0002-9551-5474>  
 Micol Eleonora Fiori <http://orcid.org/0000-0002-1813-7035>  
 Giorgio Stassi <http://orcid.org/0000-0002-1016-9059>

#### REFERENCES

- Siegel RL, Miller KD, Jemal A. Cancer statistics, 2019. *CA: A Cancer Journal for Clinicians* 2019;69:7–34.
- Dagogo-Jack I, Shaw AT. Tumour heterogeneity and resistance to cancer therapies. *Nat Rev Clin Oncol* 2018;15:81–94.
- Russo M, Siravegna G, Blaszkowsky LS, et al. Tumor heterogeneity and lesion-specific response to targeted therapy in colorectal cancer. *Cancer Discov* 2016;6:147–53.
- Dienstmann R, Mason MJ, Sinicrope FA, et al. Prediction of overall survival in stage II and III colon cancer beyond TNM system: a retrospective, pooled biomarker study. *Ann Oncol* 2017;28:1023–31.
- Van Cutsem E, Cervantes A, Adam R, et al. ESMO consensus guidelines for the management of patients with metastatic colorectal cancer. *Annals of Oncology* 2016;27:1386–422.
- Mei ZB, Duan CY, Li CB, et al. Prognostic role of tumor PIK3CA mutation in colorectal cancer: a systematic review and meta-analysis. *Ann Oncol* 2016;27:1836–48.
- Misale S, Di Nicolantonio F, Sartore-Bianchi A, et al. Resistance to anti-EGFR therapy in colorectal cancer: from heterogeneity to convergent evolution. *Cancer Discov* 2014;4:1269–80.
- Siravegna G, Mussolin B, Buscarino M, et al. Erratum: clonal evolution and resistance to EGFR blockade in the blood of colorectal cancer patients. *Nat Med* 2015;21:827.
- De Roock W, Claes B, Bernasconi D, et al. Effects of KRAS, BRAF, NRAS, and PIK3CA mutations on the efficacy of cetuximab plus chemotherapy in chemotherapy-refractory metastatic colorectal cancer: a retrospective Consortium analysis. *Lancet Oncol* 2010;11:753–62.
- Tricker EM, Xu C, Uddin S, et al. Combined EGFR/MEK Inhibition Prevents the Emergence of Resistance in EGFR -Mutant Lung Cancer. *Cancer Discov* 2015;5:960–71.
- Arena S, Siravegna G, Mussolin B, et al. MM-151 overcomes acquired resistance to cetuximab and panitumumab in colorectal cancers harboring EGFR extracellular domain mutations. *Sci Transl Med* 2016;8:324ra14.
- Van Emburgh BO, Arena S, Siravegna G, et al. Acquired Ras or EGFR mutations and duration of response to EGFR blockade in colorectal cancer. *Nat Commun* 2016;7:13665.
- Kopetz S, Desai J, Chan E, et al. Phase II Pilot Study of Vemurafenib in Patients With Metastatic BRAF -Mutated Colorectal Cancer. *Journal of Clinical Oncology* 2015;33:4032–8.
- Ahronian LG, Sennott EM, Van Allen EM, et al. Clinical Acquired Resistance to RAF Inhibitor Combinations in BRAF -Mutant Colorectal Cancer through MAPK Pathway Alterations. *Cancer Discov* 2015;5:358–67.
- Prahallad A, Heynen GJJE, Germano G, et al. Ptpn11 is a central node in intrinsic and acquired resistance to targeted cancer drugs. *Cell Rep* 2015;12:1978–85.
- Kopetz S, McDonough SL, Morris VK, et al. Randomized trial of irinotecan and cetuximab with or without vemurafenib in BRAF -mutant metastatic colorectal cancer (SWOG 1406). *Journal of Clinical Oncology* 2017;35:520.
- Corcoran RB, André T, Tretya CE, et al. Combined BRAF, EGFR, and MEK Inhibition in Patients with BRAF<sup>V600E</sup> -Mutant Colorectal Cancer. *Cancer Discov* 2018;8:428–43.
- Douillard J-Y, Oliner KS, Siena S, et al. Panitumumab-FOLFOX4 Treatment and RAS Mutations in Colorectal Cancer. *New England Journal of Medicine* 2013;369:1023–34.
- Kavuri SM, Jain N, Galimi F, et al. Her2 activating mutations are targets for colorectal cancer treatment. *Cancer Discov* 2015;5:832–41.
- Zhang L, Castanaro C, Luan B, et al. ERBB3/HER2 signaling promotes resistance to EGFR blockade in head and neck and colorectal cancer models. *Mol Cancer Ther* 2014;13:1345–55.
- Sun C, Hobor S, Bertotti A, et al. Intrinsic resistance to MEK inhibition in KRAS mutant lung and colon cancer through transcriptional induction of ErbB3. *Cell Rep* 2014;7:86–93.
- Personeni N, Fieus S, Piessevaux H, et al. Clinical Usefulness of EGFR Gene Copy Number as a Predictive Marker in Colorectal Cancer Patients Treated with Cetuximab: A Fluorescent *In Situ* Hybridization Study. *Clinical Cancer Research* 2008;14:5869–76.
- Siena S, Sartore-Bianchi A, Marsoni S, et al. Targeting the human epidermal growth factor receptor 2 (HER2) oncogene in colorectal cancer. *Annals of Oncology* 2018;29:1108–19.
- Kapitanovic S, Radosev S, Kapitanovic M, et al. The expression of p185(HER-2/neu) correlates with the stage of disease and survival in colorectal cancer. *Gastroenterology* 1997;112:1103–13.
- Sartore-Bianchi A, Trusolino L, Martino C, et al. Dual-Targeted therapy with trastuzumab and lapatinib in treatment-refractory, KRAS codon 12/13 wild-type, HER2-positive metastatic colorectal cancer (HERACLES): a proof-of-concept, multicentre, open-label, phase 2 trial. *Lancet Oncol* 2016;17:738–46.
- Liu Q, Kulak MV, Borchering N, et al. A novel HER2 gene body enhancer contributes to HER2 expression. *Oncogene* 2018;37:687–94.
- Wang Q, Tan R, Zhu X, et al. Oncogenic K-ras confers SAHA resistance by up-regulating HDAC6 and c-myc expression. *Oncotarget* 2016;7:10064–72.
- Sears R, Nuckolls F, Haura E. Multiple Ras-dependent phosphorylation pathways regulate Myc protein stability. *Genes Dev* 2000;14:2501–14.
- Yeh E, Cunningham M, Arnold H, et al. A signalling pathway controlling c-myc degradation that impacts oncogenic transformation of human cells. *Nat Cell Biol* 2004;6:308–18.
- Diosdado B, van de Wiel MA, Terhaar Sive Droste JS, et al. Mir-17-92 cluster is associated with 13q gain and c-myc expression during colorectal adenoma to adenocarcinoma progression. *Br J Cancer* 2009;101:707–14.
- Zeuner A, Todaro M, Stassi G, et al. Colorectal cancer stem cells: from the crypt to the clinic. *Cell Stem Cell* 2014;15:692–705.
- Todaro M, Alea MP, Di Stefano AB, et al. Colon cancer stem cells dictate tumor growth and resist cell death by production of interleukin-4. *Cell Stem Cell* 2007;1:389–402.
- Todaro M, Gaggianesi M, Catalano V, et al. Cd44V6 is a marker of constitutive and reprogrammed cancer stem cells driving colon cancer metastasis. *Cell Stem Cell* 2014;14:342–56.
- Cagnol S, Rivard N. Oncogenic KRAS and BRAF activation of the MEK/ERK signaling pathway promotes expression of dual-specificity phosphatase 4 (DUSP4/MKP2) resulting in nuclear ERK1/2 inhibition. *Oncogene* 2013;32:564–76.
- Lim K-H, Ancrile BB, Kashatus DF, et al. Tumour maintenance is mediated by eNOS. *Nature* 2008;452:646–9.
- Veschi V, Mangiapane LR, Nicotra A, et al. Targeting chemoresistant colorectal cancer via systemic administration of a BMP7 variant. *Oncogene* 2020;39:987–1003.
- Roux PP, Shahbazian D, Vu H, et al. Ras/Erk signaling promotes site-specific ribosomal protein S6 phosphorylation via RSK and stimulates cap-dependent translation. *J Biol Chem* 2007;282:14056–64.
- Gera JF, Mellingshoff IK, Shi Y, et al. AKT Activity Determines Sensitivity to Mammalian Target of Rapamycin (mTOR) Inhibitors by Regulating Cyclin D1 and c- myc Expression. *J Biol Chem* 2004;279:2737–46.
- He L, Thomson JM, Hemann MT, et al. A microRNA polycistron as a potential human oncogene. *Nature* 2005;435:828–33.
- Falchook GS, Long GV, Kurzrock R, et al. Dabrafenib in patients with melanoma, untreated brain metastases, and other solid tumours: a phase 1 dose-escalation trial. *The Lancet* 2012;379:1893–901.
- Hong DS, Morris VK, El Osta B, et al. Phase IB Study of Vemurafenib in Combination with Irinotecan and Cetuximab in Patients with Metastatic Colorectal Cancer with BRAF<sup>V600E</sup> Mutation. *Cancer Discov* 2016;6:1352–65.
- Schütte M, Risch T, Abdavi-Azar N, et al. Molecular dissection of colorectal cancer in pre-clinical models identifies biomarkers predicting sensitivity to EGFR inhibitors. *Nat Commun* 2017;8:14262.
- Linnekamp JF, Hooff SRvan, Prasetyanti PR, et al. Consensus molecular subtypes of colorectal cancer are recapitulated in vitro and in vivo models. *Cell Death Differ* 2018;25:616–33.
- Vermeulen L, De Sousa E Melo F, van der Heijden M, et al. Wnt activity defines colon cancer stem cells and is regulated by the microenvironment. *Nat Cell Biol* 2010;12:468–76.
- Siravegna G, Mussolin B, Buscarino M, et al. Clonal evolution and resistance to EGFR blockade in the blood of colorectal cancer patients. *Nat Med* 2015;21:795–801.
- Segaert S, Van Cutsem E. Clinical signs, pathophysiology and management of skin toxicity during therapy with epidermal growth factor receptor inhibitors. *Annals of Oncology* 2005;16:1425–33.



## SUPPLEMENTAL INFORMATION

### METHODS

#### CRC sphere cell culture

Purification and propagation of sphere cells was assessed as previously described<sup>1</sup> from 60 primary tumor specimens (age range 40–80 years) from CRC patients undergoing colon resection, in accordance with the ethical standards regarding Human Experimentation (authorization CE9/2015, Policlinico Paolo Giaccone, Palermo) (online supplemental table 1). CSphCs were cultured in serum-free stem cell medium (SCM) supplemented with EGF and b-FGF. Authentication of CSphC lines was routinely performed using a short tandem repeat DNA profiling kit (GlobalFiler™ PCR kit, Applied Biosystem) following the manufacturer's instructions and analyzed by ABI PRISM 3130 (Applied Biosystem). CSphC DNA profiles were matched with their relative patient tumor tissues. Mycoplasma presence was assessed with the MycoAlert™ Plus Mycoplasma Detection Kit (Lonza) every 3 months. To assess *ErbB2* copy number in CR-CSphCs we analyzed DNA samples using Digital Droplet PCR (Bio-Rad). After droplet generation and PCR amplification, plates were loaded in a Bio-Rad QX200 droplet reader and analyzed using the QuantaSoft v1.7.4 software (Bio-Rad) to evaluate droplets positive for *ErbB2* and/or *Rpp30*. Negative (no DNA) and positive (*ErbB2* amplified SKBR3 established cell line) controls were included in each plate. An *ErbB2/Rpp30* ratio < 1.25 identified non-amplified samples.<sup>2,3</sup> The mutational profiles of the CSphCs were assessed by using a custom NGS panel and sequencing data were generated by MiSeq platform (Illumina).

#### CRC sphere cell treatment

CSphCs were treated with vemurafenib 1 μM (S1267, Selleckchem), cetuximab 20 μg/ml and trastuzumab 10 μg/ml (kindly provided by the Department of Central Hospital Services- Policlinico Paolo Giaccone), taselisib 0.5 μM (GDC-0032, Chemietek), BKM120 1 μM (S2247, Selleckchem), trametinib 100 nM (S2673, Selleckchem), cobimetinib 0.5 μM (S8041, Selleckchem) or miransertib 2 μM (S8339, Selleckchem). All the drugs were added in culture media every 48 hours.

The primary human CAF cell lines were isolated from CRC tissues obtained in accordance with the ethical policy of the University of Palermo Committee on Human Experimentation. For co-culture experiments,  $1 \times 10^5$  immortalized CAFs (CAFs) were plated as monolayer into 12-well plates for 48 hours, until confluence was reached and subsequently  $6 \times 10^5$  GFP-transduced CSphCs were seeded in presence or absence of HGF (1 μg/ml, MAB294, R&D), OPN (2 μg/ml, AF1433, R&D) and SDF-1 (50 μM, A5602, Sigma-Aldrich) neutralizing antibodies. After 48 hours cells were treated with 0.5 μM of taselisib for additional 72 hours. The preparation of CAF conditioned medium (CAF CM) was performed by culturing  $1 \times 10^6$  cells in 5 ml of SCM for 48 hours. To analyze *ErbB2*

expression levels, CSphCs were exposed to CAF CM, HGF (100 ng/ml, PeproTech), OPN (1 µg/ml, Sigma-Aldrich) and SDF-1 (100 ng/ml, PeproTech) for 48 hours.

### **Cell survival**

Cell proliferation and viability were evaluated by using CellTiter-Glo® Luminescent Cell Viability Assay Kit (Promega) according to the manufacturer's instructions and analyzed by Infinite® F500 (Tecan). Tripan blue exclusion test was accomplished to validate cell viability. CSphC death was assessed by adding Hoechst 33342 (Thermo Fisher Scientific) or 7-AAD (BD Pharmingen) and analyzed by a fluorescence microscope or flow cytometer, respectively.

### **Reverse-Phase Protein microArrays**

The RPPA assay was carried out by the Functional Proteomics RPPA Core Facility by MD Anderson (Houston, TX, USA)<sup>4</sup> on a service basis (online supplemental table 4). The data analysis was performed by our group. Briefly, cell pellets were lysed for protein extraction by resuspension in a buffer containing T-PER reagent (Thermo Fisher Scientific), 300 mM NaCl (J.T.Baker; Avantor Performance Materials, Center Valley, PA), protease and phosphatase inhibitor cocktails (Sigma-Aldrich), followed by 20 min incubation on ice. Following protein extraction, samples underwent centrifugation at 10,000xg for 10 minutes and, subsequently, supernatants were transferred to fresh tubes for quantification of total protein concentration (Bradford reagent method, Thermo Fisher Scientific). Before shipping for RPPA assay service, lysates were diluted to a final concentration of 0.5 µg/µl using 2X sodium dodecyl sulfate (SDS) buffer (Thermo Fisher Scientific) and 2-mercaptoethanol was added to a final concentration of 2.5%. Analysis of pre-normalized RPPA data was performed by means of the "R3.6" software and the following packages: 'base', 'coin', 'exactRankTests', 'gridExtra', 'grid', 'tidyverse', 'plyr', 'dendextend' and 'ComplexHeatmap'.

### **Western blot**

Cell were lysed in presence of ice-cold buffer containing Tris-HCL 10 mM (Sigma-Aldrich), NaCl 50 mM (Sigma-Aldrich), sodium pyruvate 30 mM (Sigma-Aldrich), NaF 50 nM (Sigma-Aldrich), ZnCl<sub>2</sub> 5 µM (Sigma-Aldrich), triton 1% (Bio-Rad), protease inhibitor cocktail (Sigma-Aldrich), phosphatase inhibitor cocktail 2 and 3 (Sigma-Aldrich), sodium orthovanadate 0.1 nM (Sigma-Aldrich), sodium butyrate 10 mM (Sigma-Aldrich) and PMSF 1 mM (Sigma-Aldrich). Proteins extracted were loaded in SDS-PAGE gels and blotted on nitrocellulose membranes. After incubation with blocking solution (0.1% Tween 20 and 5% non-fat dry milk in PBS) for 1 hour at room

temperature, membranes were exposed overnight at 4°C to HER3/ErbB3 XP (D22C5, rabbit IgG, CST), HER2/ErbB2 XP (D8F12, rabbit IgG, CST), EGF receptor XP (D38B1, rabbit IgG, CST), phospho-AKT XP (Ser473; D9E, rabbit, IgG, CST), AKT (rabbit polyclonal, CST), phospho-GSK3 $\alpha/\beta$  (Ser21/9; D17D2, rabbit IgG, CST), GSK-3 $\beta$  (27C10, rabbit IgG, CST), phospho-ERK 1/2 (Thr202/Tyr204; rabbit polyclonal, CST), ERK 1/2 (137F5, rabbit IgG, CST), Myc (rabbit polyclonal, CST), phospho-MEK1/2 (Ser217/221; 41G9, rabbit IgG, CST) or MEK1/2 (rabbit polyclonal, CST).  $\beta$ -actin (8H10D10, mouse, CST) was used as loading control to normalize protein expression. Primary antibodies were revealed using anti-mouse or anti-rabbit HRP-conjugated (goat H+L, Thermo Fisher Scientific) for 1 hour at room temperature and detected with SuperSignal™ West Dura Extended Duration Substrate (Thermo Fisher Scientific) using Amersham imager 600 (GE Healthcare). Protein levels were calculated by densitometric analysis using ImageJ software.

### **Cytokines quantification**

CAF-released cytokines involved in tumor inflammation, cell proliferation and immune response processes were quantified using the Bio-Plex Pro™ Human Cytokine 21-plex and 27-plex Assay (Bio-Rad). HGF, OPN, SDF-1 and TGF- $\beta$  production was assessed by using the Human Cancer Biomarker Panel 1 16-plex #171AC500M, Bio-Plex Pro Human Cytokine SDF-1 $\alpha$  Set #171B6019M, and Bio-Plex Pro™ TGF- $\beta$  3-plex Assay #171W4001M, respectively. Raw data were analyzed by Bio-Plex Software (Bio-Rad).

### **Flow cytometry and cell sorting**

Cells were harvested, washed in PBS twice and stained for 1 hour at 4°C with conjugated antibodies CD44v6-APC (2F10, mouse IgG1, R&D systems) or isotype matched control (IC002A, mouse IgG1, R&D systems) and analyzed using both Accuri C6 Plus and FACSLyric (BD) flow cytometers. CD90 expression was assessed by using CD90 purified antibody (5E10, mouse IgG1k, BD) or isotype matched control (MOPC-21, mouse IgG1k, BD) and subsequent labeling with secondary antibodies Alexafluor 647 (goat anti-mouse IgG1, Thermo Fisher Scientific). Enrichment of CD44v6 or OFP expressing cells was accomplished by FACSMelody cell sorter. Prior to sorting, cells were washed with PBS containing 2% BSA and 2 mM EDTA and filtered with a 70  $\mu$ M mesh to prevent clogging. Post-sorting acquisition was performed in order to verify the population purity. Dead cells were excluded on the basis of the uptake of 7-AAD (0.25  $\mu$ g/1x10<sup>6</sup> cells, BD Biosciences).



### RNA Extraction, Real-Time PCR and RNASeq

Total RNA of CSphCs was isolated by using Trizol Reagent (Thermo Fisher) and retro-transcribed with the high-capacity c-DNA reverse Transcription kit (Applied Biosystem). Real-time PCR was performed by using the rotor gene probe PCR master mix (Qiagen) and the following primers: *ErbB2* (Hs01001580\_m1), *ErbB3* (Hs00176538\_m1), *Egfr* (Hs01076078\_m1) and *Gapdh* (Hs02786624\_g1) (Applied Biosystem). The relative mRNA level was normalized to *Gapdh* and calculated by using the comparative Ct method ( $\Delta\Delta Ct$ ).

To evaluate the miRNA expression profiles of CSphCs untreated and exposed to different treatments, total RNA samples were retro-transcribed and real time PCR were performed using Megaplex pools kit (Applied Biosystem) specific for a set of 384 microRNAs (TaqMan Human MicroRNA Array A) as recommended by manufacturer's instructions. Collected data were analyzed with the Thermo FisherCloud software.

NEBNext Ultra Directional RNA Library Prep Kit for Illumina was used for the preparation of RNASeq samples following the manufacturer's instructions. mRNA was purified using oligo-dT magnetic beads from total RNA. Retrotranscribed cDNA was used for ligation with adapters and PCR amplification. Clustering and DNA sequencing was assessed using the Illumina NextSeq 500. Analysis was performed by using the Illumina data analysis pipeline RTA v2.4.11 and Bcl2fastq v2.17. Raw sequencing reads were aligned to Ensembl release 84 (GRCh38 assembly) using the HISAT2 2.1.0 pipeline. Data were analyzed using the R version 3.5.0 and plotted by the pheatmap version 1.0.10, gtools 3.8.1 and ggplot2 3.0.0. Gene set enrichment analysis (GSEA) was assessed by selecting Hallmarks and canonical pathways within molecular signatures database (MSigDB) version 7.0. False Discovery Rate  $q$  value  $\leq 0.05$  was used to identify significantly enriched gene sets.

### Chromatin immunoprecipitation (ChIP) and ChIP-qPCR

Chromatin was isolated from both CD44v6<sup>+</sup> and CD44v6<sup>-</sup> CSphCs, IMEC, IMEC-MYC and IMEC-MYC-PI3K cells. Cells were fixed adding formaldehyde directly to the cell culture media to reach a final concentration of 1%, then were incubated for 10 min at room temperature (RT). The reaction was quenched adding glycine to a final concentration of 125 mM and incubated 5 min at RT. The medium was removed and cells were washed 3 times with cold, sterile PBS plus protease inhibitor, then cells were collected by centrifugation at 4°C for 5 min at 1200 rpm. ChIP experiments were performed as previously described.<sup>5, 6</sup> Briefly, cell pellets were lysed in lysis buffer (50 mM Tris-HCl pH 8, 0.1% SDS, 10 mM EDTA pH 8, 1 mM PMSF (Sigma-Aldrich), protease inhibitor cocktail (Roche)) and chromatin was sonicated with a Bioruptor Pico sonicator

(Diagenode) for 25 cycles of 30 s, to reach an average fragment size of ~ 300 kb. Following quantification, 10 µg of sonicated chromatin were used in each immune-precipitation and incubated overnight at 4°C with 4 µg of indicated antibodies: anti- monomethyl histone H3 Lys4 (rabbit polyclonal, Abcam); anti-acethyl histone H3 Lys27 (rabbit polyclonal, Abcam). Concomitantly, protein G-coupled Dynabeads (Thermo Fisher Scientific) were blocked overnight at 4°C with 1 mg/ml sonicated salmon sperm DNA (Thermo Fisher Scientific) and 1 mg/ml BSA and then incubated with the ChIP reactions for 4 hours at 4°C. Magnetic beads were sequentially recovered and resuspended in RIPA buffer (10 mM Tris-HCl, pH 8, 0.1% SDS, 1 mM EDTA, pH 8, 140 mM NaCl, 1% DOC, 1% Triton, 1 mM PMSF, protease inhibitor cocktail), washed 5 times with ice-cold RIPA buffer, twice with ice-cold RIPA-500 buffer (10 mM Tris-HCl, pH 8, 0.1% SDS, 1 mM EDTA, pH 8, 500 mM NaCl, 1% DOC, 1% Triton, 1 mM PMSF, protease inhibitor cocktail), twice with ice-cold LiCl buffer (10 mM Tris-HCl, pH 8, 0.1% SDS, 1 mM EDTA, pH 8, 250 mM LiCl, 0.5% DOC, 0.5% NP-40, 1 mM PMSF, protease inhibitor cocktail) and once with TE buffer (10 mM Tris-HCl, pH 8, 1 mM EDTA, pH 8, 1 mM PMSF, protease inhibitor cocktail). Finally, the crosslinking was reversed in direct elution buffer (10 mM Tris-HCl, pH 8, 0.5% SDS, 5 mM EDTA, pH 8, 300 mM NaCl) at 65°C overnight and DNA was purified using Agencourt AMPure XP SPRI beads (Beckman, #A63882) and dissolved in 60 µl of Tris-HCl, pH 8. DNA was analyzed by quantitative PCR using the 2x SensiFAST SYBR No-ROX Mix (Bioline). The following oligos were used: Prom1 (fwd: CACCATCATGTGTGCGCCAAG / rev: GCAGGTTGGAAGAGGCAAAA), ENH2 (fwd: CAGTTTGTGGCCTGGACATC / rev: TACCTACTTCACCAGCCAGC), Prom2 (fwd: GGCTTGGGATGGAGTAGGAT / rev: AAATTCCCTAGGCTGCCACT), ENH1 (fwd: GACCACCAGAGTCCAGAGAG / rev: TCTCCGAACAAAAGGGACCA), HGE (fwd: GATCCGGAAGTACACGATGC / rev: GGCTGGGAGGACTTCACC), control (fwd: GATCAAGTCAGGCTGAATACACG / rev: TCTGTGCTCCTAGCTTGTCCT). All experimental values were shown as percentage of input. To take into account background signals, we subtracted the values obtained with a non-immune serum to the relative ChIP signals.

### CRISPR editing and lentiviral transduction

CSphCs were transfected with 1 µg of all-in-one OFP vector system for CRISPR-based genome editing (Thermo Fisher Scientific) and 1 µg of pMA-T plasmid containing customized donor DNA for *Pik3ca*<sup>E545K</sup> (Thermo Fisher Scientific), using the X-tremeGENE HP DNA Transfection Reagent (Roche) according to the manufacturer's instructions. DNA from control and transfected CSphCs was purified using the DNeasy Blood & Tissue Kit (Qiagen). The presence of *Pik3ca*<sup>E545K</sup> mutation

was assessed using the HotStarTaq Plus Master Mix Kit (Qiagen) using the following primer set: F-ATTGTTCACTACCATCCTC; R-TAATGTGCCAACTACCAATG. Amplified products were then purified using the MinElute PCR Purification Kit (Qiagen). Purification and base pair sequence were prepared using the BigDye Terminator v3.1 Cycle Sequencing Kit and BigDye X-Terminator Purification Kit (Applied Biosystems), respectively. Capillary electrophoresis was performed on ABI PRISM 3130 Genetic Analyzer.

Lentiviral particles were generated by transfecting HEK-293T packaging cells with p-TWEEN LUC-GFP plasmids together with psPAX2 (Addgene, 12260) and pMD2.G (Addgene, 12259) in DMEM 10% FBS supplemented with XtremeGENE HP DNA Transfection Reagent (Roche). For stable cell transduction, concentrated lentiviral particles were added to  $1 \times 10^5$  cells in culture medium in the presence of 8  $\mu\text{g}/\text{mL}$  of polybrene (Sigma-Aldrich). hTERT-immortalized human mammary epithelial cells (IMEC) were transduced with pMXs-c-Myc, PGK-Pik3ca H1047R, pBABE-puro-Ras V12, and MSCV-p53DD-iGFP vector, respectively as previously described.<sup>6</sup> CAFs immortalization has been performed using a pLV-hTERT-IRES-hygro lentiviral plasmid (Addgene). Hygromycin (10  $\mu\text{g}/\text{ml}$ ; ant-hg-5, Invivogen) was used for selection of CAFs.

### Animals and tumor models

6-8 weeks old male NOD/SCID mice were purchased by Charles River Laboratories and housed in the animal house at the Department of Biomedicine, Neuroscience and Advanced Diagnostics (Bi.N.D., University of Palermo). Mice were kept in a barrier facility for animals in a temperature-controlled system with a 12 hours dark/light cycle. Mice were given *ad libitum* access to pelleted chow [Special Diets Services-811900 VRF1 (P), Essex, UK] and to 0.45 mm filtered tap water in sterile drinking bottles. Each cage (1284L, Tecniplast S.p.A., Italy) provided with radiation-sterilized bedding (SAWI Research Bedding, JELU-WERK, Germany) has been used to house a maximum of 6 mice. Enrichment material such as soft paper and small red plastic houses (The Mouse House, ACRE011, Tecniplast) was used to meet animal welfare. All the surgical procedures have been performed during daytime, in accordance with the animal care committee guidelines of the University of Palermo (Italian Ministry of Health authorization n. 154/2017-PR). Subcutaneous xenografts were generated by injecting  $2.5 \times 10^5$  CSphCs in the flank of NOD/SCID mice, in 150  $\mu\text{l}$  of 1:1 SCM/Matrigel (BD) solution. After tumor appearance (0.03-0.06  $\text{cm}^3$ ), mice were randomized in control and treatment groups (6 mice/group). Mice were treated for 5 days/week, for 4 weeks, with vehicle, tselisib (5 mg/Kg, once-daily, oral gavage), vemurafenib (20 mg/Kg, twice-daily, oral gavage), trastuzumab (5 mg/Kg, once-weekly, *i.p.*), cetuximab (40 mg/Kg, twice-weekly, *i.p.*), BKM120 (20 mg/Kg, once-daily, oral gavage), trametinib (0.3 mg/Kg, once-daily, oral

gavage) or cobimetinib (5 mg/Kg, once-daily, oral gavage). Tumors were measured twice per week by a digital caliper. Tumor volume was calculated using the formula: largest diameter x (smallest diameter)<sup>2</sup> x  $\pi/6$ . Once the endpoints were reached (2 cm in tumor diameter or when mice showed signs of suffering), animals were sacrificed accordingly to Directive 2010/63/EU guidelines (D.lgs 26/2016) and organs were collected for subsequent analyses. For the adjuvant therapy experiments,  $3 \times 10^5$  LUC-transduced *Kras*-mutant CSphCs resuspended in PBS were injected into the spleen of NOD/SCID mice. The migration of sphere cells was assessed at the time of cell injection and at 30 min immediately after splenectomy up to 12 weeks (every 4 weeks) following *i.p.* injection of VIVO Glo<sup>TM</sup> Luciferin (150 mg/kg, Promega) by using *in vivo* imaging system (IVIS Spectrum, PerkinElmer). After 5 days of sphere cells injection, mice were treated for 3 weeks with vehicle or taselisib.

### **Immunofluorescence/Immunohistochemistry**

Cytospun of CD44v6<sup>+</sup> and CD44v6<sup>-</sup> cell fractions were fixed and permeabilized as previously described.<sup>1</sup> Cells were exposed overnight at 4°C to specific antibodies to detect CD44v6 (2F10, mouse IgG<sub>1</sub>, R&D systems) and HER2 (D8F12, rabbit IgG, CST). Subsequently, cells were labeled with secondary antibodies, Rhodamine Red-x Goat anti-Mouse IgG1 and Alexa Fluor-488 Goat anti-rabbit IgG (Life Technologies). Nuclei were counterstained using TOTO-3 iodide (Life Technologies). Cells were examined under a confocal microscope. For CAF-CSphC co-culture experiment, cells were labeled with CD90 (SE10, mouse IgG1, BD Pharmingen) and subsequently with Alexa Fluor-647 Goat anti-mouse IgG1 (Life Technologies). Nuclei were counterstained using Hoechst (33258, Thermofisher). Cell staining were examined by using EVOS Cell Imaging System (Life Technologies).

Immunohistochemical and immunofluorescence analysis were performed on 5- $\mu$ m-thick paraffin-embedded xenograft sections using antibody specific for CD44v6 (2F10, mouse IgG<sub>1</sub>, R&D systems), HER2 (D8F12, rabbit IgG, CST), phospho-AKT XP (Ser473; D9E, rabbit, IgG, CST), Ki67 (T595, IgG1<sub>k</sub>, Novocastra) and CK20 (Ks20.8, IgG2a<sub>k</sub>, Novocastra). Stainings were then revealed using byotyne-streptavidine system (Dako) and detected with 3-amino-9-ethylcarbazole (AEC, Dako). Nuclei were counterstained with aqueous hematoxylin (Sigma-Aldrich). Azan-Mallory and H&E stainings were performed using standard protocols.



### Statistical analysis

Results are shown as mean  $\pm$  SD for at least three repeated independent experiments for each group. The mean and SD were obtained by analyzing replicates using Prism 5 (GraphPad Software, La Jolla, CA, USA) applying ANOVA test (one-way or two-way) with Bonferroni multiple comparisons test. P-values less than 0.05 were considered statistically significant. \*indicates  $P < 0.05$ , \*\* indicates  $P < 0.01$  and \*\*\* indicates  $P < 0.001$ . RNA-seq data were normalized with log<sub>2</sub>-counts per million transformation. Differential expression analyses between diverse conditions were conducted in R (v3.6.1) by using limma package. P-values for log<sub>2</sub> fold-change values are corrected with Benjamini-Hochberg procedure, only statistically significant differences were reported. ggplot2 and pheatmap packages were used for plotting the distributions and line plots, and heatmaps with clustergrams and sample annotations, respectively.

## SUPPLEMENTAL FIGURE LEGENDS

### Supplementary Figure 1. CD44v6 positive cells express high levels of HER2 and MAPK-ERK signaling molecules.

(A) Dose-response of cetuximab (Cmab) on *Ras/Braf*-wt (CSphC#14, 21) and *Braf*-mutant (CSphC#2, 5) sphere cell lines at the indicated time points. Data are mean  $\pm$  S.D. of 3 independent experiments. (B) Waterfall plot of cetuximab response in *Ras/Braf*-wt xenograft tumors from sensitive CSphCs treated for 4 weeks and analyzed 1 week after treatment suspension. *Braf*- and *Kras*-mutant xenografts served as control. (C) Unsupervised clustering of RNA-seq data from sphere cells sensitive and resistant to cetuximab and harboring the indicated mutations. (D) Log fold change (logFC) values of a subset of statistically differentially expressed genes, involved in the MAPK pathway, in sensitive versus resistant *Ras/Braf*-wt sphere cells to cetuximab, obtained by limma analysis. (E) Statistical distribution of CD44v6 positivity in 47 CSphC lines characterized by the indicated mutational background. Boxes and whiskers represent median  $\pm$  S.D. of 6 experiments. Dotted lines indicate high ( $\geq 70\%$ ), medium (69%-31%) and low ( $\leq 30\%$ ) CD44v6 levels. (F) (*Left panel*) Representative immunohistochemical analysis for CD44v6 on tumor xenografts generated by the injection of *Ras/Braf*-wt (CSphC#14) sphere cells and treated with cetuximab for 4 weeks. Scale bars, 200  $\mu$ m. (*Right panel*) Percentage of CD44v6 positivity in tumor xenografts generated by the injection of *Ras/Braf*-wt (CSphC#14, 21, 33) sphere cells. Data are mean  $\pm$  S.D. of 3 independent experiments. (G) RPPA analysis of CRC spheres (Bulk) and enriched CD44v6<sup>+</sup> and CD44v6<sup>-</sup> *Braf*- (CSphC#2) mutant cells. (H) Immunoblot analysis of HER3, HER2 and EGFR and their relative bar graphs on CD44v6<sup>-</sup> and CD44v6<sup>+</sup> cells derived from 10 different CR-CSphC lines with different mutational backgrounds (CSphC#1, #2, #3, #9, #11, #15, #16, #21, #33, #37).  $\beta$ -actin was used as loading control. Data are mean  $\pm$  S.D. of 3 independent experiments performed with 10 different sphere cell lines. (I) Bar graphs of immunoblot band densities for HER2 on enriched CD44v6<sup>+</sup> and CD44v6<sup>-</sup> *Ras/Braf*-wt, *Braf*- and *Kras*- mutant cells. Data are mean  $\pm$  S.D. of 3 independent experiments performed in *Ras/Braf*-wt (CSphC#14, 21, 33), *Braf*- (CSphC#1, 2, 3, 5) and *Kras*- (CSphC#8, 11, 16) mutant CD44v6 fractions. (J) Immunofluorescence analysis for HER2 and CD44v6 on CD44v6<sup>+</sup> and CD44v6<sup>-</sup> in *Ras/Braf*-wt (CSphC#21), *Braf*- (CSphC#2) and *Kras*- (CSphC#11) mutant cells. Nuclei were counterstained with TOTO-3. Data are representative of 2 independent experiments performed with *Ras/Braf*-wt (CSphC#14, 21), *Braf*- (CSphC#2, 5) and *Kras*- (CSphC#8, 11) mutant sphere cells. Scale bars, 10  $\mu$ m. (K) Browser view of RNA-seq analysis on *Braf*-mutant CD44v6 positive (green) and negative (red) CSphCs. The tracks of expression (RPKM normalized) for *ERRB2* (*Upper panel*) and *Gapdh* (*Lower panel*) are shown. For each cell type, tracks of three different biological replicates are shown.

### Supplementary Figure 2. PI3K activation is associated with increased *ErbB2* transcription levels.

(A) Unsupervised clustering of RNA-seq data from CD44v6<sup>high</sup> (>70%) and CD44v6<sup>low</sup> (<30%) cells. (B) LogFC values of a subset of statistically differentially expressed genes, enriched for PI3K pathway, in CD44v6<sup>high</sup> vs CD44v6<sup>low</sup> cells. Data were computed by limma package in R. (C) (*Upper panels*) Schematic diagram of OFP CRISPR Nuclease and donor DNA (pMA-T) vectors. (*Lower panels*) Electropherograms showing the DNA sequence of *Pik3ca*-wt low expressing HER2 CR-CSphC lines (CSphC#23, 5, 15), following targeted genome editing. Red stars indicate the newly introduced point mutation (red letters G $\rightarrow$ A). crRNA=CRISPR RNA; tracr=trans-activating crRNA; Pol III=terminator. (D) Bar graphs of immunoblot band densities for HER2, pAKT and AKT on *Ras/Braf*-wt (CSphC#6, 23), *Braf*- (CSphC#2, 5), *Kras*- (CSphC#10, 15) mutant cells and their corresponding CRISPR/Cas9-*Pik3ca*<sup>E545K</sup> cells. Data are mean  $\pm$  S.D. of 3 independent experiments performed with the indicated CSphCs. (E) ChIP-qPCR for the histone marks H3K27Ac using amplicons for 2 promoters (Prom1 and Prom2), 3 potential enhancer regions (Enh1, Enh2, and HGE) and negative control (Control) in IMEC, IMEC-MYC and IMEC-MYC-PI3K cells. Enrichment is indicated as % of input. (F) Percentage of viable CD44v6 low ( $\leq 30\%$ ),

medium (31-69%) and high ( $\geq 70\%$ ) cells treated with miransertib, BKM120 and taselisib for 72 hours. Boxes and whiskers represent median  $\pm$  S.D. of 3 experimental replicates of 29 CR-CSphC lines. (G) Percentage of cell viability in 29 CR-CSphC lines, harboring the indicated mutations, exposed to different doses of PI3K and AKT inhibitors as indicated. Boxes and whiskers represent median  $\pm$  S.D. of 3 experimental replicates of 29 CR-CSphC lines. (H) Percentage of cell viability of CD44v6<sup>+</sup> and CD44v6<sup>-</sup> *Braf*<sup>-</sup> (CSphC#2, 3, 4, 5) and *Kras*<sup>-</sup> (CSphC#8, 9, 10, 11, 16) mutant sphere cells treated with BKM120. Data are mean  $\pm$  S.D. from 3 independent experiments. (I) mRNA expression levels of *ErbB2* in CSphCs and CD44v6<sup>+</sup> enriched cells treated as indicated for 48 hours. Data are mean  $\pm$  S.D. of 3 independent experiments performed with *Ras/Braf*-wt (CSphC#14, 33), *Braf*<sup>-</sup> (CSphC#1, 5) and *Kras*<sup>-</sup> (CSphC#10, 11) mutant sphere cell lines. (J) *ErbB2* mRNA expression levels in CSphCs treated with vehicle or taselisib in presence of CAF CM. Data are mean  $\pm$  S.D. of 3 independent experiments using *Ras/Braf*-wt (CSphC#7, 27), *Braf*<sup>-</sup> (CSphC#2, 3) and *Kras*<sup>-</sup> (CSphC#12, 20) mutant sphere cell lines. (K) *ErbB2* mRNA expression levels in tumor xenografts treated with vehicle or BKM120 for 4 weeks. Mice were sacrificed 1 weeks after treatment suspension. Data are means  $\pm$  S.D. of 6 mice per group injected with *Ras/Braf*-wt (CSphC#14, 21, 33), *Braf*<sup>-</sup> (CSphC#1, 2, 5) or *Kras*<sup>-</sup> (CSphC#8, 11, 16) mutant sphere cells. (L) Representative immunofluorescence analysis for HER2 on tumor xenografts generated by the injection of *Braf*<sup>-</sup> (CSphC#2) mutant sphere cells and treated as in K. Nuclei were counterstained with Toto-3 (blue color). Scale bars, 20  $\mu$ m.

**Supplementary Figure 3. Triple targeting of HER2, MEK and PI3K overcomes the protective effect mediated by CAF-released cytokines.** (A) Size of xenograft tumors generated by subcutaneous injection of *Braf*<sup>-</sup> (CSphC#1, 2, 3, 5) and *Kras*<sup>-</sup> (CSphC#8, 11, 16) mutant cells, treated for 4 weeks as indicated and monitored up to 10 weeks. "I" indicates the time of cell injection. Time-point 0 indicates the start of treatment. Data are mean  $\pm$  S.D. of 3 independent experiments (n=6 mice per group). (B) RPPA analysis of *Ras/Braf*-wt (CSphC#14), *Braf*<sup>-</sup> (CSphC#2) and *Kras*<sup>-</sup> (CSphC#11) mutant cells treated with vehicle or vemurafenib (Vemu) in combination with trastuzumab (Tmab) and PI3K inhibitor (BKM120) (VTB). Total and phosphorylated S6 are indicated. (C) Relative band densities of immunoblots for pAKT, AKT, pGSK, GSK3, pERK, ERK and Myc in tumor xenografts-derived cells of mice injected with *Ras/Braf*-wt (CSphC#14, 21, 33), *Braf*<sup>-</sup> (CSphC#1, 2, 3), *Kras*<sup>-</sup> (CSphC#8, 11, 16) mutant sphere cells treated with vehicle (Vehicle) or vemurafenib (Vemu) in combination with trastuzumab (Tmab) and PI3K inhibitor (BKM120) (V+T+B). Data are expressed as mean  $\pm$  S.D. of 3 subcutaneously implanted CSphC lines for each mutational status (n= 6 mice per group). (D) (Left panel) Representative average of miRNAs equivalent CT values on tumor xenograft-derived cells isolated from mice injected with *Kras*<sup>-</sup> (CSC#8) mutant CR-CSphCs treated with vehicle (Vehicle) or vemurafenib in combination with trastuzumab plus PI3K inhibitor (Vemu+Tmab+BKM120). (Right panel) Clustergrams of miRNAs expression levels of those indicated with arrows in the correlation plot. Data are representative of 3 independent experiments performed with 3 different CR-CSphCs (CSC#8, 11, 16). (E) Bar graphs of immunoblot relative band densities for pAKT, AKT, pGSK, GSK, pERK, ERK and Myc in *Ras/Braf*-wt, *Braf*<sup>-</sup> and *Kras*<sup>-</sup> mutant sphere cells treated with vehicle (Vehicle) or trastuzumab (Tmab) in combination with trametinib (MEKi) and PI3K inhibitor (BKM120) (T+Mi+B). Data are mean  $\pm$  S.D. of 3 independent experiments performed with *Ras/Braf*-wt (CSphC#14, 21, 33), *Braf*<sup>-</sup> (CSphC#1, 2, 3) and *Kras*<sup>-</sup> (CSphC#8, 11, 16) mutant sphere cultures. (F) RPPA analysis of *Braf*<sup>-</sup> (CSphC#2) and *Kras*<sup>-</sup> (CSphC#11) mutant cells treated with vehicle or trastuzumab (Tmab) in combination with trametinib (MEKi) and PI3K inhibitor (BKM120) (TMiB) for 24 hours. Total and phosphorylated S6 expression levels are indicated. (G) Heatmap of viability percentage of cells with the indicated mutational background treated with vehicle (Vehicle) or trastuzumab in combination with MEKi and BKM120 (T+Mi+B) for 72 and 120 hours. Data are the mean of 3 experimental replicates performed on 30 cell lines. (H) (Left panel) Representative average of miRNAs equivalent CT values on *Kras*<sup>-</sup> (CSC#11) mutant CR-

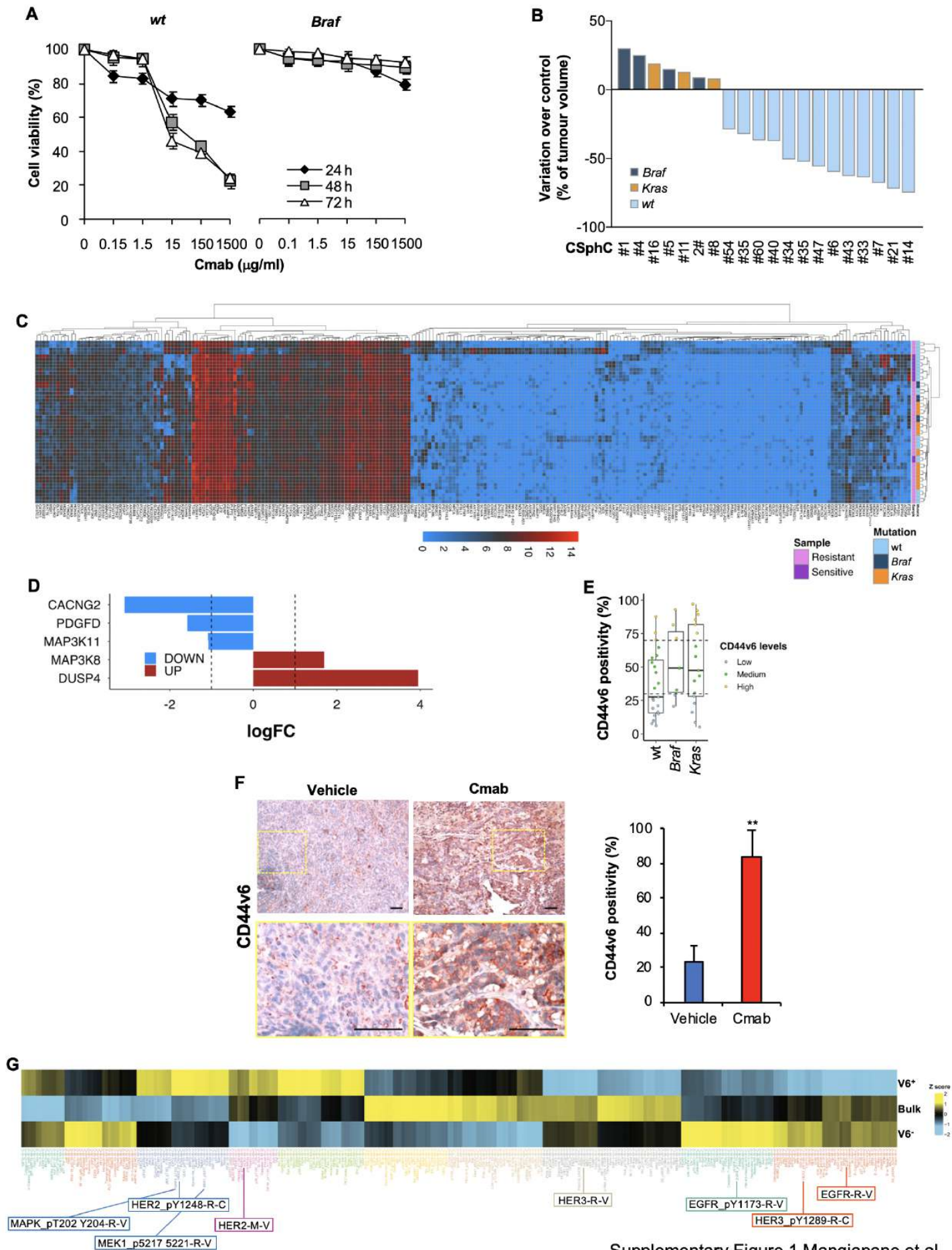
CSphCs, exposed to the indicated therapeutic regimen combinations. Before treating with trastuzumab in combination with MEK inhibitor and BKM120 (Tmab+MEKi+BKM120) for 24 hours, cells were pre-treated with vemurafenib in combination with trastuzumab and BKM120 for 5 days and maintained for 2 days off-drug period. (*Right panel*) Clustergrams of miRNAs expression levels, indicated with arrows in the correlation plot. Data are representative of 3 independent experiments performed with different CR-CSphCs (CSC#8, 11, 16). (**I**) Bar graphs of immunoblot relative band densities for pAKT, AKT, pMEK, MEK, pERK, ERK and Myc in *Braf*<sup>-</sup> (#1, 2, 3) *Kras*<sup>-</sup> (CSphC#8,11, 16) mutant sphere cells treated with vehicle (Vehicle) or vemurafenib (V) in combination with trastuzumab (T) and BKM120 (V+T+B) or trastuzumab in combination with MEKi and BKM120 (T+Mi+B) and cultured in FBS-free DMEM or CAF CM for 24 hours. Data are expressed as mean  $\pm$  S.D. of 3 independent experiments. (**J**) Growth of cells previously untreated (Vehicle) or treated with vemurafenib in combination with trastuzumab and BKM120 (Pre-treated V+T+B) for 5 days and exposed to trastuzumab in combination with MEKi and BKM120 (T+Mi+B) or V+T+B. Data are expressed as mean  $\pm$  S.D. of 4 independent experiments performed with 15 CR-CSphCs with different mutational backgrounds.

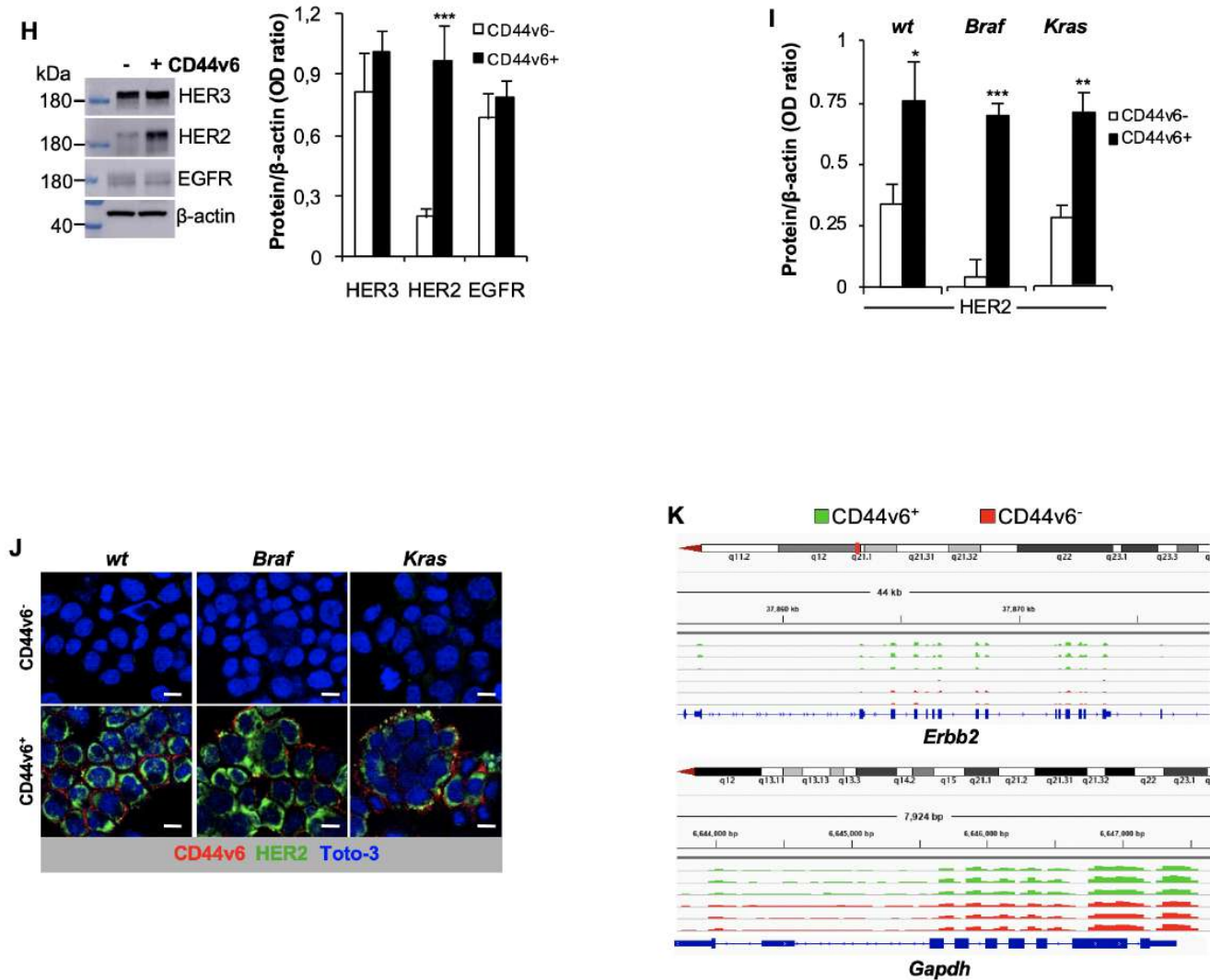
**Supplementary Figure 4. The triple targeting of MEK, HER2 and PI3K induces regression of xenograft tumors generated by the injection of CR-CSCs.** (**A**) Subcutaneous size of tumor xenografts generated by sphere cell lines bearing the indicated mutational background and treated as indicated. Time-point “I” indicates cell injection and 0 the start of treatment. Data are mean  $\pm$  S.D. of 3 independent experiments (n=6 mice per group). (**B**) H&E and immunohistochemical analysis of CD44v6, Ki67 and CK20 on tumor xenografts generated by the injection of *Braf*<sup>-</sup> (CSphC#2) mutant sphere cells. Mice were treated for 4 weeks with vehicle (Vehicle) or trastuzumab (Tmab) plus trametinib (MEKi) plus BKM120 (BKM120). (**C**) Evaluation of CD44v6 positivity by flow cytometry in CR-CSphCs obtained from *Ras/Braf*-wt, *Braf*<sup>-</sup> and *Kras*<sup>-</sup> mutant xenografts treated as indicated, and analyzed 2 weeks after treatment suspension. Data are expressed as mean  $\pm$  S.D. of 3 independent experiments performed with *Ras/Braf*-wt (CSphC#21, 24, 33), *Braf*<sup>-</sup> (CSphC#2, 3, 5) and *Kras*<sup>-</sup> (CSphC#8, 11, 13) mutant cells. (**D**) Cell viability of the indicated sphere cells exposed for 72 and 120 hours to trastuzumab (Tmab) in combination with cobimetinib (Cob) and taselisib (Tas). Data are expressed as mean  $\pm$  S.D. of 4 independent experiments. (**E**) Subcutaneous outgrowth of *Kras*<sup>-</sup> (CSphC#8, 9, 11, 13) mutant sphere cell-derived xenograft tumors at the indicated weeks and treated with vehicle (Vehicle) or trastuzumab (Tmab) in combination with cobimetinib (Cob) and taselisib (Tas) for 4 weeks. Data are means  $\pm$  S.D. of tumor size for each cell line (n= 6 mice per group). “I” indicates the time of cell injection and 0 the start of treatment. (**F**) CD44v6 flow cytometry analysis on cells dissociated from tumor xenografts treated as in (E). Grey histograms represent the relative isotype matched control. (**G**) Representative azan mallory staining and immunohistochemical analysis of CD44v6, CK20 and Ki67 on tumor xenografts obtained from the injection of *Kras*<sup>-</sup> (CSphC#9, 11) mutant sphere cells treated as indicated. Scale bars, 100  $\mu$ m.



## REFERENCES

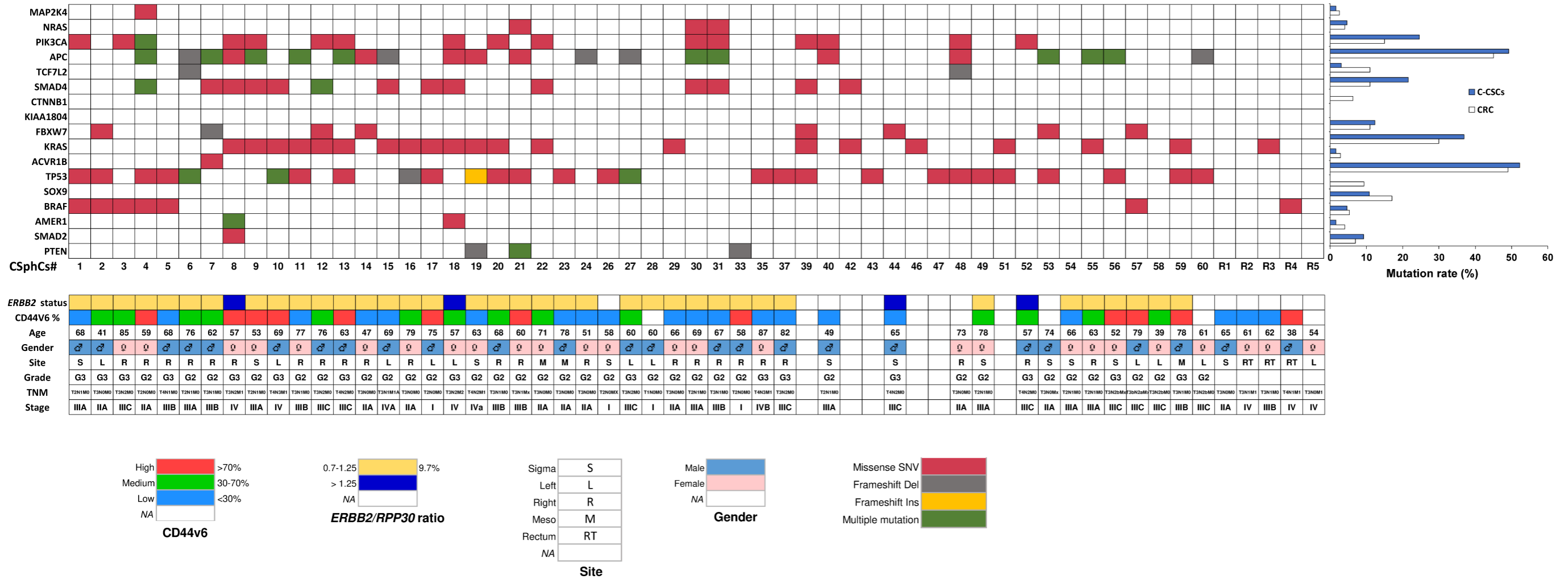
- 1 Todaro M, Alea MP, Di Stefano AB, Cammareri P, Vermeulen L, Iovino F, *et al.* Colon cancer stem cells dictate tumor growth and resist cell death by production of interleukin-4. *Cell stem cell* 2007;**1**:389-402.
- 2 Gevensleben H, Garcia-Murillas I, Graeser MK, Schiavon G, Osin P, Parton M, *et al.* Noninvasive detection of HER2 amplification with plasma DNA digital PCR. *Clinical cancer research : an official journal of the American Association for Cancer Research* 2013;**19**:3276-84.
- 3 Takegawa N, Yonesaka K, Sakai K, Ueda H, Watanabe S, Nonagase Y, *et al.* HER2 genomic amplification in circulating tumor DNA from patients with cetuximab-resistant colorectal cancer. *Oncotarget* 2016;**7**:3453-60.
- 4 Li J, Zhao W, Akbani R, Liu W, Ju Z, Ling S, *et al.* Characterization of Human Cancer Cell Lines by Reverse-phase Protein Arrays. *Cancer cell* 2017;**31**:225-39.
- 5 Fagnocchi L, Cherubini A, Hatsuda H, Fasciani A, Mazzoleni S, Poli V, *et al.* A Myc-driven self-reinforcing regulatory network maintains mouse embryonic stem cell identity. *Nature communications* 2016;**7**:11903.
- 6 Poli V, Fagnocchi L, Fasciani A, Cherubini A, Mazzoleni S, Ferrillo S, *et al.* MYC-driven epigenetic reprogramming favors the onset of tumorigenesis by inducing a stem cell-like state. *Nature communications* 2018;**9**:1024.





Supplementary Figure 1 Mangiapane et al.

**Supplementary Table 1.** Cancer sphere cells and their mutational profiles, ERBB2 status and CD44v6 expression.



COSMIC-reported mutation of the analyzed genes (*upper panel*). Mutation types (missense SNV, frameshift deletion or insertion, and multiple mutations) are indicated. Percentage of mutation rate in CRC patients reported in TGCA database (white bars) and in C-CSCs (blue bars) are indicated on the right. ERBB2 status and CD44v6 expression of CSphCs and clinical data related to CRC patients are reported (*lower panel*).



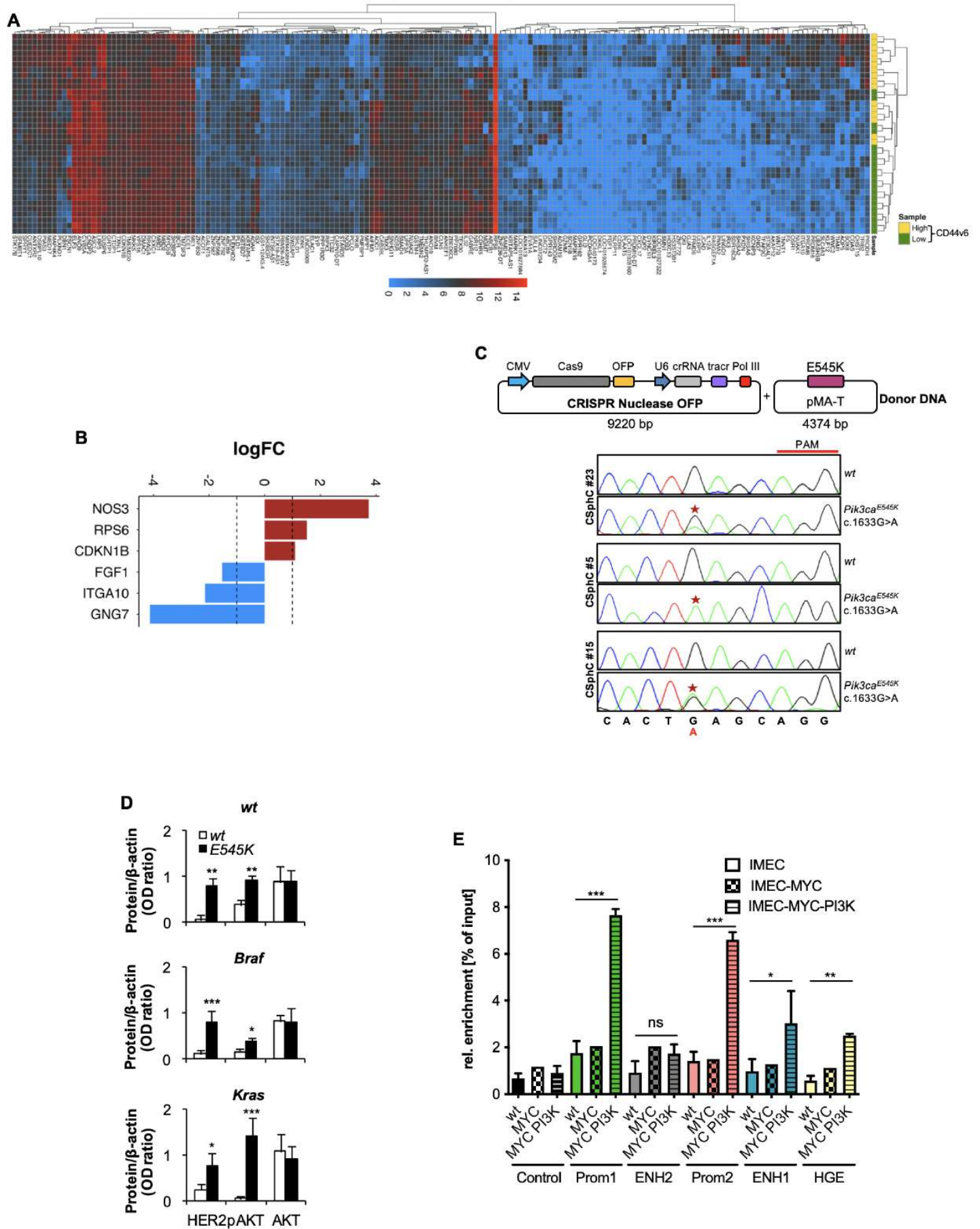
Table with columns for Gene, Resistant, Sensitive, and various sub-categories (KRAS, BRAF, WT, etc.) for both cell types. The table lists numerous genes and their corresponding expression values across different markers.

Table with 100 columns and 1000 rows of numerical data. The first column contains labels (e.g., 1209A, 1209B, 1209C) and the remaining columns contain numerical values. The data is organized into a grid-like structure with varying column widths.

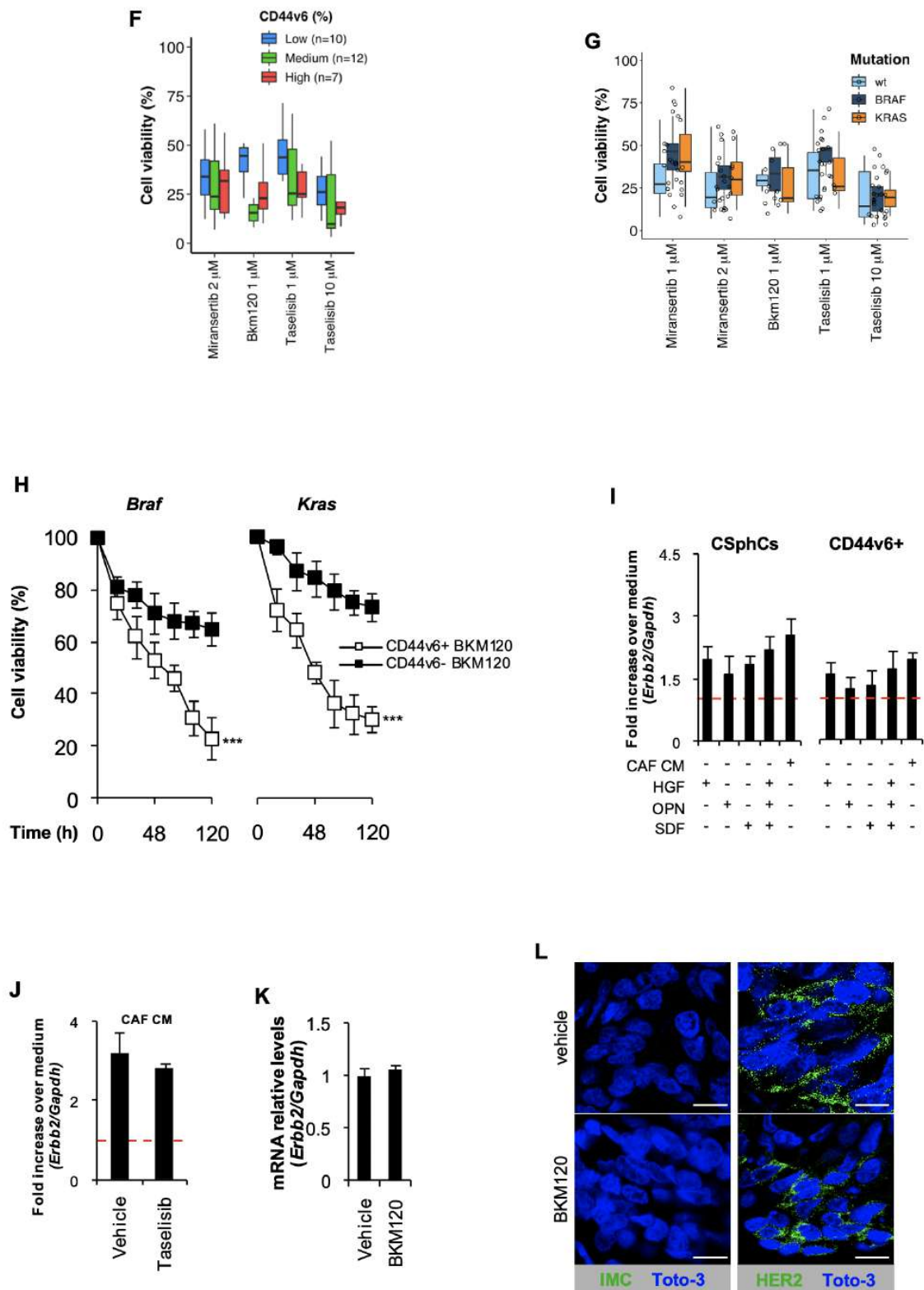








Supplementary Figure 2 Mangiapane et al.



Supplementary Figure 2 Mangiapane et al.

Supplemental Table 3. Statistically differentially expressed genes in CD44<sup>hi</sup> vs CD44<sup>lo</sup> cells.

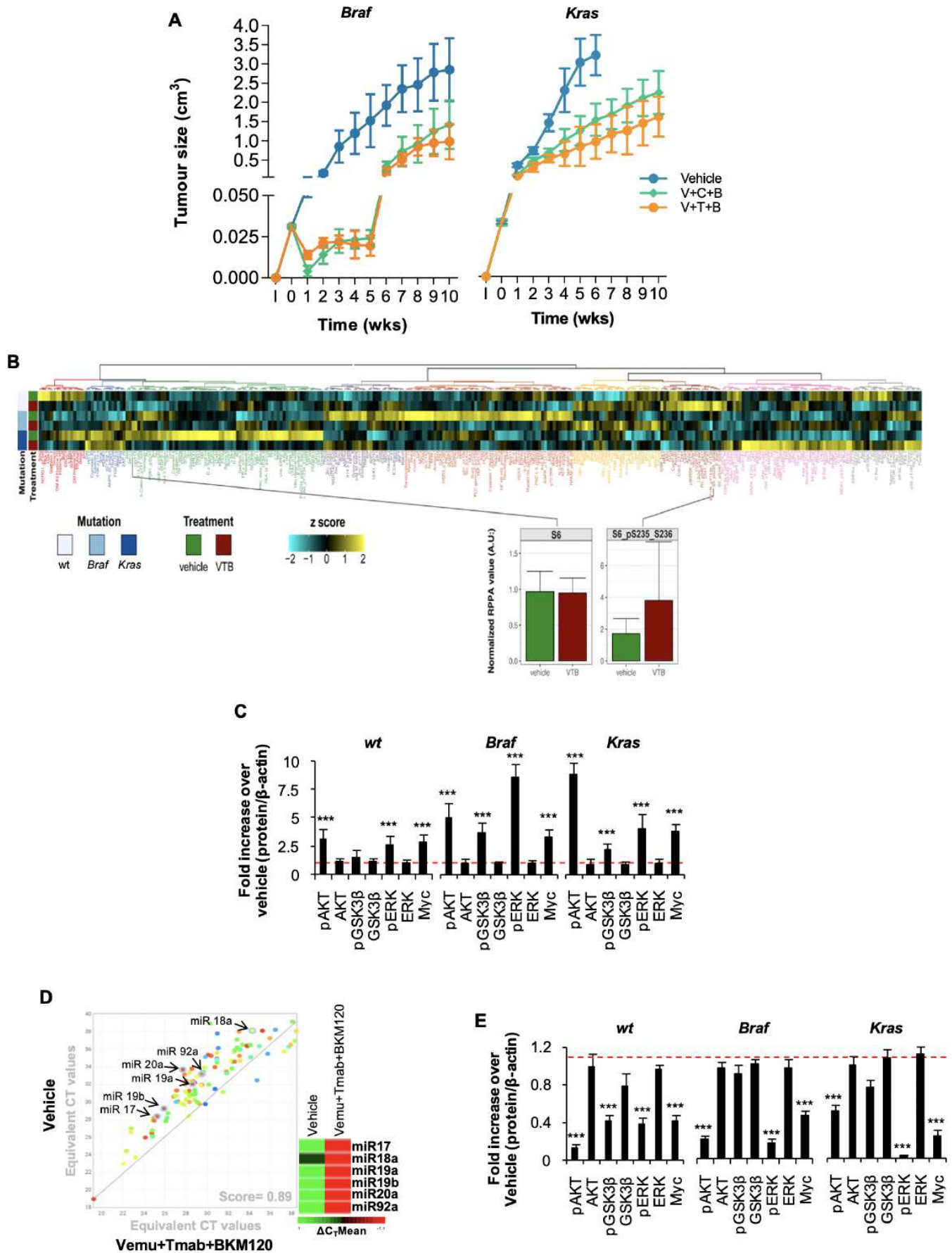
Table with columns for Gene, High, Low, and various statistical values (Log2FC, P, FDR, etc.) for each gene. The table lists numerous genes such as SH3BP5, FOS, LOC401702, and many others, with their corresponding expression data across different conditions.

Table with 4 columns: Gene/Region, Chr, Start, End. Lists genomic coordinates for various genes including TM6X, STKB17, GPR43, ANKRD1, CAPN10, ZNF502, UFSB, SMN1, ACSB9, DYN11, ULBP3, GALNT3, ZEB1L2, LRPS, MID2, RPS6, RIPK3, PLXND1, TNN1, FSCN1, ZNF36-DT, CAD, AIFM3, PKDX, ZNF202, MIM2, GS1-12K45, TMSF3, MKK3, MAP4K4, GZMM, ELF3, PLAA23, PLAGL2, TME2M30, CUCD1, NR12, ZNF792, KDSR, PPP1R3D, RASGEF1B, LOC101927, EVAT1, RASGEF1B, MAP3K15, BCR, OSR1, IL3, ANKFF1, NLRP1, KRTPAS-A1, GRTP1, VPS16, CGAS, MARK1, FMPF3, KBTBD7, ST3GAL1, BVM, CY5A, TTC32, CDN1B, SWAP1, PRDM16, FTGL1.

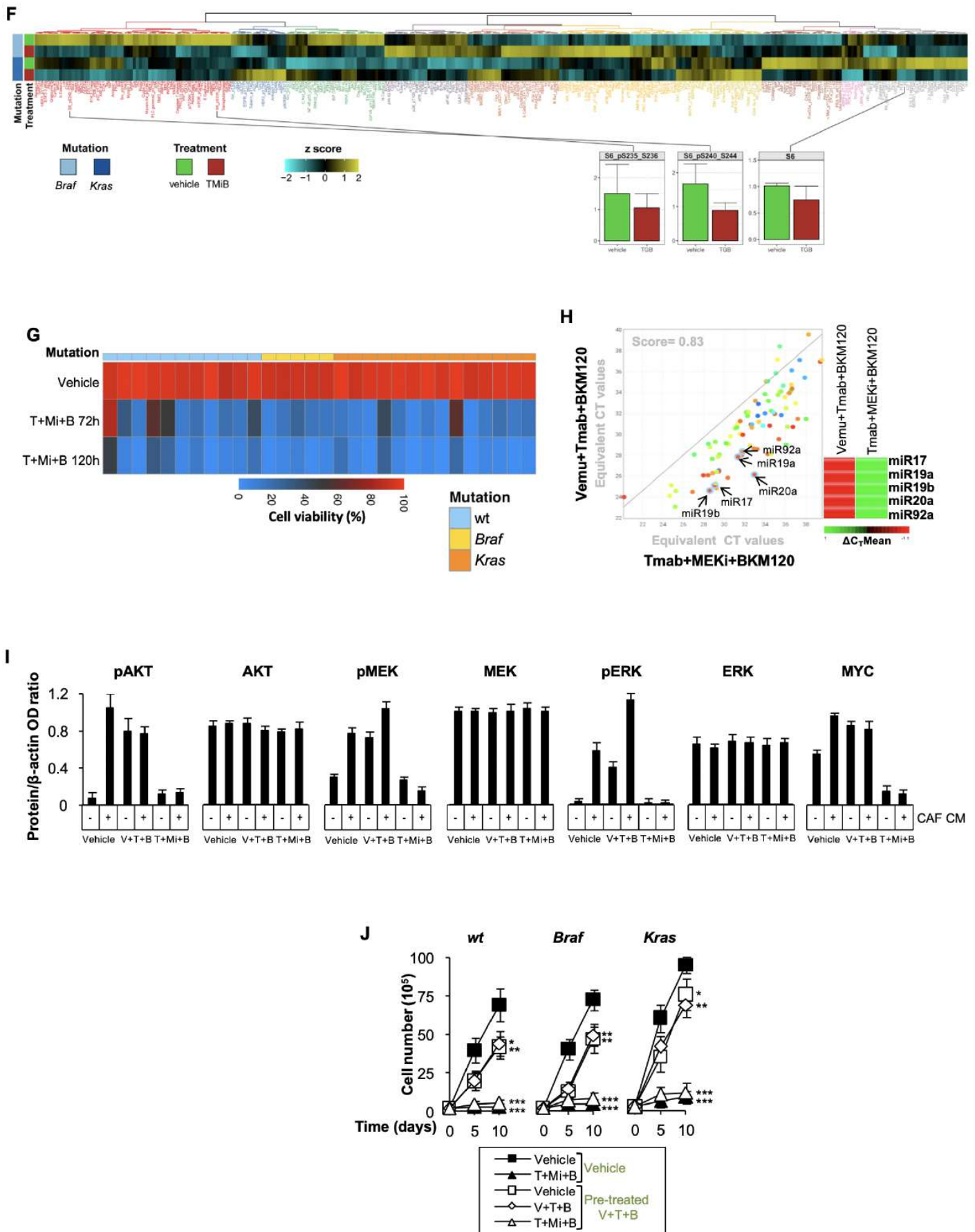


Gene	logFC	AveExpr	t	P.Value	adj.P.Val	B
SHISA6	-6.89870189	1.950197	-16.3044265	6.64E-11	1.44E-06	13.2263035
F5	-5.98865649	2.96825621	-11.6081004	7.35E-09	4.56E-05	9.8886489
FRMD6	-5.37781882	1.88885254	-11.555572	7.81E-09	4.56E-05	9.84094619
LOC440173	-2.19996893	0.54999223	-11.4904469	8.43E-09	4.56E-05	9.78141911
TFAP2C	-4.17150142	1.15926421	-10.40154	3.18E-08	0.00013774	8.71975856
ABCB1	7.26216532	7.71477681	9.33979736	1.29E-07	0.00046666	7.5526942
GLI2	-5.05003206	1.41809754	-9.17754864	1.62E-07	0.00050072	7.36180863
AQP5	-8.22905877	4.18878574	-8.98657014	2.12E-07	0.00057282	7.13263306
MBD1	1.19900121	9.2159608	8.82246496	2.67E-07	0.00064315	6.93175532
MPP1	5.69004741	5.27115897	8.68177849	3.27E-07	0.0007089	6.75658619
LINC00909	2.32291245	6.06656678	8.59717004	3.70E-07	0.0007288	6.64990754
GABRE	4.76709454	7.26087774	8.41194588	4.86E-07	0.00087706	6.41282585
CTDP1	1.3251893	8.42809785	7.96245828	9.57E-07	0.0015943	5.81681014
LINGO1	-5.12275412	2.02857441	-7.85985378	1.12E-06	0.00165937	5.67655876
LINC01234	-5.45129611	2.75309823	-7.76700857	1.30E-06	0.00165937	5.54827785
SHLD1	1.82622551	5.75168719	7.74973831	1.33E-06	0.00165937	5.5242718
PRDM8	-6.56391285	2.91625888	-7.74664245	1.34E-06	0.00165937	5.51996369
ISX	6.06143201	6.61193395	7.54846766	1.83E-06	0.00208196	5.24113641
TXN1	1.12007982	8.90262	7.47880838	2.04E-06	0.00218251	5.14169027
HOXC13	-2.9199932	0.95424778	-7.4560739	2.12E-06	0.00218251	5.10907146
SHROOM2	-4.86148093	2.47773826	-7.40375614	2.30E-06	0.00220459	5.03370195
NOS3	3.73482395	6.18544548	7.39307771	2.34E-06	0.00220459	5.01826608
FGF1	-1.53523411	0.45122185	-7.31472762	2.66E-06	0.00239736	4.90046439
CAB39L	3.72376131	7.69951067	7.13895401	3.54E-06	0.00306496	4.64564891
PRDM16-DT	-3.42034115	1.41036369	-7.02355195	4.28E-06	0.00356491	4.4730705
AOAH	5.97428541	5.890468	6.95379118	4.81E-06	0.0038548	4.36771982
CLN5	1.55983309	7.23625125	6.91869144	5.10E-06	0.00394135	4.31441983
SMAD4	1.20166919	8.02901666	6.8697541	5.53E-06	0.00406092	4.2397786
PNMA2	-5.68896275	2.70065466	-6.85966334	5.63E-06	0.00406092	4.22434016
DKK1	-1.40472307	0.42275256	-6.78677905	6.36E-06	0.00435374	4.11234611
KIRREL3	-4.42294272	2.02836833	-6.78001836	6.44E-06	0.00435374	4.10191449
AOC1	5.31877341	7.77930321	6.76105974	6.65E-06	0.00435936	4.07262261
ELAC1	2.19664696	5.72628457	6.7067342	7.29E-06	0.00463957	3.98836799
IRX3	-4.45438075	1.60816458	-6.67766414	7.66E-06	0.0047356	3.94308801
UBASH3B	-5.97067964	3.2642889	-6.54886543	9.55E-06	0.00558527	3.74083538
WNT7B	-4.08348349	2.44680818	-6.52276863	9.99E-06	0.00568845	3.69953059
SAMD13	3.91537875	3.39999914	6.49776932	1.04E-05	0.0057871	3.65986012
SHISA2	-5.02188865	1.49380009	-6.47502145	1.08E-05	0.00586892	3.62367503
ADAM19	-3.28890638	1.22375277	-6.42089665	1.19E-05	0.00628966	3.53724404
SOX8	-5.54826487	2.51156081	-6.36706727	1.31E-05	0.00674381	3.45081768
PKIB	3.43821249	4.91253883	6.32617079	1.41E-05	0.0070755	3.38484467
RBM26-AS1	2.46494119	5.00974016	6.31211371	1.44E-05	0.00708722	3.36210618
PRODH	-5.03539624	5.45211088	-6.29186137	1.49E-05	0.00715913	3.32929058
WWC2	-4.13612098	2.42289182	-6.25821084	1.58E-05	0.00725109	3.27461995
AKAP12	-4.13322762	1.94277935	-6.24963249	1.61E-05	0.00725109	3.26065403
GJA3	-3.33895597	1.62016038	-6.2259285	1.68E-05	0.00725835	3.22200159
STX18-AS1	1.47224129	4.61328246	6.19519879	1.77E-05	0.00726806	3.17175888
PLEKHO2	-2.37297171	5.17702106	-6.18181207	1.81E-05	0.00726806	3.14982451
GSTM4	2.59663933	7.80176225	6.18166875	1.81E-05	0.00726806	3.14958953
ZNF772	-4.35769452	2.28250738	-6.1443299	1.94E-05	0.0076248	3.08825697
SFMBT1	-1.07303603	7.28035897	-6.08266708	2.16E-05	0.00835819	2.98648296
ECE1	-1.44779798	9.43524749	-6.03007048	2.38E-05	0.00902193	2.89919433
ME1	-1.24489659	8.66588911	-5.98273623	2.59E-05	0.00948971	2.82026365
PLD1	-2.8009986	6.52369196	-5.98273008	2.59E-05	0.00948971	2.82025337
DACT2	-5.05538336	2.96638477	-5.94964371	2.75E-05	0.00990477	2.76487068
THUMPD3-AS	2.00322489	7.37085714	5.93192536	2.83E-05	0.0099872	2.73514116
NUAK1	-4.26809332	3.79197153	-5.92689401	2.86E-05	0.0099872	2.72669007
PCLO	5.41092554	4.85086658	5.81996199	3.47E-05	0.01176059	2.54613679
TIAM1	-5.9460642	3.18615053	-5.80530469	3.57E-05	0.01176059	2.5212486
DUSP6	-3.05121781	10.0715333	-5.79943905	3.61E-05	0.01176059	2.51127931
KRTAP5-1	3.77545401	4.91732938	5.77754158	3.75E-05	0.01176059	2.47401487
IDNK	1.85978011	5.54502149	5.77649964	3.76E-05	0.01176059	2.47223987
SNHG11	1.12576917	7.53546332	5.7595998	3.88E-05	0.01176059	2.4434265
SH3BGR	1.53378955	4.53038239	5.7532041	3.92E-05	0.01176059	2.43251061
CNDP2	1.46954999	10.5249676	5.75268497	3.93E-05	0.01176059	2.4316243
ANXA13	3.86434144	3.40806077	5.75197733	3.93E-05	0.01176059	2.43041608
GPR162	-2.29991572	1.08228759	-5.74574138	3.98E-05	0.01176059	2.41976553
HS3ST3B1	-3.99820158	2.26064427	-5.73987058	4.02E-05	0.01176059	2.40973313
QKI	-5.65438155	2.79729875	-5.72746155	4.11E-05	0.01187083	2.38851021
NUAK2	1.90793219	7.52137226	5.71824457	4.18E-05	0.01191446	2.37273117
RRAGA	1.22145813	8.85012019	5.69806885	4.34E-05	0.01207733	2.33814551
MIR4458HG	4.06836452	5.02161117	5.68682401	4.43E-05	0.01207733	2.31884211
ANO9	2.68395399	10.6151688	5.68295139	4.46E-05	0.01207733	2.31218968
PIAS3	-1.36045649	7.80203461	-5.67348184	4.54E-05	0.01213802	2.2959131
KLF12	-4.69001395	2.5987819	-5.66295154	4.63E-05	0.01220912	2.27779707
CHST15	-5.23040109	2.0438753	-5.65658433	4.69E-05	0.01220912	2.26683485
ANO10	2.15842191	7.26964566	5.64363132	4.80E-05	0.01220912	2.24451489
ZNF566	-1.59489699	5.72962267	-5.61020436	5.10E-05	0.01261666	2.18679672
CXCL17	-3.26195032	1.35880461	-5.59102844	5.29E-05	0.01272156	2.15360884
SALL4	-4.20985135	1.83124486	-5.57235436	5.48E-05	0.01302502	2.12123581
MYO5B	1.32982143	9.21070332	5.53734451	5.84E-05	0.0137492	2.06040107
ASCL2	3.00896507	10.6410507	5.5070282	6.18E-05	0.01423815	2.00757276
LOC10192867	-1.26812215	0.36812549	-5.43235609	7.11E-05	0.01619831	1.87686484
GNF7	-4.12880049	1.73414798	-5.42074031	7.27E-05	0.01638248	1.85645782
CXCC1	1.11710554	9.4191657	5.40783388	7.44E-05	0.01661102	1.83375995
OSBP10	-1.38118865	8.01006792	-5.37563634	7.91E-05	0.01742214	1.77702897
TEX30	4.32849288	6.62864654	5.3150353	8.87E-05	0.01890606	1.66984114
STARD5	1.82678696	6.05604323	5.30868937	8.97E-05	0.01890606	1.65858598

LOC1019281C	-2.78739745	1.53882211	-5.30727298	9.00E-05	0.01890606	1.65607309
SCN1B	-3.07125459	0.98177489	-5.27025925	9.65E-05	0.01991119	1.59030237
PCDHGA4	-1.17682644	0.29420661	-5.26974517	9.66E-05	0.01991119	1.58938751
TRIB2	-5.61893883	3.08197761	-5.25060735	0.00010015	0.02026117	1.55530262
AQP2	-3.44316715	1.94809312	-5.24007176	0.00010218	0.02047908	1.53651623
SLC4A3	-3.75777976	3.0065658	-5.23126536	0.0001039	0.02055907	1.52080113
ZNF567	-2.04623448	5.72748846	-5.18923623	0.00011255	0.02137104	1.44564886
INTS6-AS1	1.87033795	4.22923893	5.16522358	0.00011783	0.02189936	1.40260058
ACOT1	-1.36411603	5.00467304	-5.16466968	0.00011795	0.02189936	1.40160664
SH3BP2	1.24680628	9.22897211	5.16281115	0.00011837	0.02189936	1.39827129
LOC1019278E	4.40583245	3.30437434	5.15738031	0.0001196	0.02194008	1.38852228
SYP	2.10361367	5.57711646	5.12856354	0.00012638	0.02298756	1.33672428
CDHR5	4.3042722	7.09021206	5.11895465	0.00012872	0.02307851	1.31942689
MGMT	4.45762972	7.28263203	5.10263695	0.00013281	0.02356348	1.2900236
IL12A	-1.57842949	0.69279706	-5.09168709	0.00013562	0.02386769	1.27027237
SPRY1	-1.65708645	7.37955421	-5.08347686	0.00013778	0.02405102	1.25545212
DBN1	-3.79674429	6.47669661	-5.05503582	0.00014551	0.02519803	1.20404271
TMX3	1.23868987	7.5641969	5.04985183	0.00014697	0.02524843	1.19466049
STK17B	-1.12077543	7.21521687	-5.04470006	0.00014843	0.02529905	1.18533298
GPR143	-2.95198905	1.52537127	-4.99548771	0.00016319	0.0267614	1.0960534
KCNIP3	-3.27554818	2.27338778	-4.98900989	0.00016525	0.02682975	1.08427763
ANTXR2	-2.69349491	6.89521402	-4.97430629	0.00017001	0.02725902	1.05752806
CAPN10-DT	2.10062314	5.86639852	4.93420081	0.00018372	0.02847998	0.98442266
SDR16C5	-3.2260709	1.32466703	-4.93296172	0.00018416	0.02847998	0.9821607
MED17	-1.07981933	7.81703762	-4.92347137	0.00018758	0.02847998	0.96482945
DMAC1	1.6141531	8.83615942	4.92322235	0.00018767	0.02847998	0.96437453
ZNF850	-1.830786	5.27651452	-4.92317654	0.00018769	0.02847998	0.96429085
UPF3A	1.39279413	7.98762036	4.92191609	0.00018815	0.02847998	0.9619881
SMN1	2.45929355	2.59552225	4.91440761	0.00019091	0.02869693	0.94826645
ABCB9	-1.71028129	6.48571732	-4.8922912	0.00019928	0.02954501	0.9078072
DYNC111	-3.86800701	1.68587244	-4.88700078	0.00020134	0.02964708	0.89811983
ULBP3	-2.96917364	2.25518615	-4.88148821	0.0002035	0.02976383	0.88802191
GALNT5	2.88106225	5.34826486	4.86161858	0.00021152	0.03072855	0.85159298
ZBED6CL	1.86476656	7.39554535	4.84758908	0.00021737	0.03136863	0.82584155
LRP5	-1.23534821	10.8780622	-4.8285357	0.0002256	0.03212655	0.79082958
MBD2	1.52288767	9.19029692	4.8171599	0.00023066	0.03255552	0.76990435
RPS6	1.51954191	13.9394349	4.81503039	0.00023162	0.03255552	0.76598547
RIPK3	2.27260357	5.71014589	4.81089306	0.00023349	0.03260764	0.75837004
PLXND1	-4.18660184	6.44948687	-4.78720191	0.00024455	0.03393262	0.71472248
TNNT1	-3.56826748	3.05210917	-4.77421429	0.00025084	0.03458343	0.69076581
FSCN1	-6.94214738	6.59076611	-4.74821862	0.00026393	0.03615799	0.64275409
ZNF236-DT	1.59284998	3.26668834	4.73547628	0.0002706	0.03683885	0.61919082
JCAD	-2.2858179	0.81882003	-4.73031429	0.00027335	0.03689488	0.60963974
AIFM3	3.68321833	7.24011199	4.72832415	0.00027442	0.03689488	0.60595662
PXDN	-5.7829441	2.78852944	-4.71527349	0.00028153	0.03761782	0.58179247
TMEM42	1.46421949	6.86511569	4.67330718	0.00030573	0.04035222	0.5039554
G51-124K5.4	2.20084619	4.42737506	4.66471855	0.00031094	0.04079104	0.48800078
TM75F3	-1.09952003	9.61668084	-4.65779187	0.0003152	0.0411018	0.47512741
MKKS	1.07182729	9.0378199	4.64448021	0.00032358	0.04148482	0.45037226
MAP4K4	-1.87022311	8.2873717	-4.62986384	0.00033303	0.04148482	0.42316798
GZMM	-2.06544875	1.23942908	-4.62882017	0.00033372	0.04148482	0.42122458
ELF3	1.76600294	11.2059059	4.62731361	0.00033471	0.04148482	0.41841902
PLAAT5	-3.22033217	1.53402257	-4.61228921	0.00034478	0.04198779	0.39042645
TMEM230	1.15918736	8.94262603	4.60340097	0.00035088	0.04243078	0.37385476
CUEDC1	-2.27839198	6.88172981	-4.59794929	0.00035468	0.0426517	0.36368611
NR1I2	4.9785876	6.68181643	4.59415131	0.00035735	0.0427354	0.35660009
ZNF792	-1.69405006	5.96824551	-4.58195094	0.00036606	0.04325261	0.3338269
CD96	-3.11994829	1.02416863	-4.580234	0.00036731	0.04325261	0.33062078
KDSR	1.21364309	7.90490793	4.5797434	0.00036767	0.04325261	0.32970459
PPP1R3D	1.7290905	5.8856795	4.5699012	0.00037489	0.0437546	0.31131919
RASGEF1A	-3.09092452	1.38516867	-4.56457254	0.00037886	0.0438548	0.30136084
LOC1019273Z	2.16397452	2.16138729	4.55131077	0.00038894	0.0445305	0.27656386
EVA1A	5.51609268	4.13706951	4.54961821	0.00039024	0.0445305	0.27339775
PP7080	2.52484631	7.50288574	4.54432657	0.00039435	0.0445305	0.26349728
MAP3K15	-1.68981942	0.61368671	-4.54258117	0.00039572	0.0445305	0.26023106
BCR	-1.44120814	9.25807198	-4.53859002	0.00039886	0.0445305	0.25276109
OSR1	-4.12552237	3.800022	-4.53500761	0.0004017	0.0445305	0.24605473
IL32	5.33888817	7.40159429	4.53167788	0.00040436	0.0445305	0.23982019
ANKEF1	1.23663083	6.98297141	4.53095326	0.00040494	0.0445305	0.23846328
NLRP11	-2.20805807	0.85866666	-4.53038666	0.00040539	0.0445305	0.23740222
KRTAP5-AS1	3.21090457	2.97479175	4.52978045	0.00040588	0.0445305	0.23626696
GRTP1	1.15393359	8.55145433	4.52796777	0.00040734	0.0445305	0.23287208
VPS16	1.11210794	8.77851702	4.52000256	0.00041383	0.04470061	0.21795044
CGAS	-2.91527082	5.94422265	-4.51702682	0.00041627	0.04470061	0.21237417
MARK1	4.51841599	3.93805934	4.51514268	0.00041783	0.04470061	0.20884298
PMFBP1	2.57971577	5.47226891	4.51348291	0.00041921	0.04470061	0.205732
KBTBD7	3.58828146	5.67694377	4.50816051	0.00042366	0.04480021	0.19575408
ST3GAL1	-4.24203523	2.61283559	-4.50741878	0.00042428	0.04480021	0.19436334
BIVM	1.32975882	7.5239564	4.4952983	0.00043461	0.04507416	0.17162941
CYBSA	1.51495998	10.1988496	4.49461033	0.00043521	0.04507416	0.17033857
TTC32	1.36695082	6.05389601	4.48639081	0.00044237	0.04538161	0.15491252
CDKN1B	1.09045764	8.57389574	4.47033869	0.00045671	0.04641244	0.12476713
SWSAP1	1.45241657	5.50012109	4.46628169	0.0004604	0.04656963	0.11714418
PRDM16	-4.56068759	3.96493007	-4.45483686	0.000471	0.04737476	0.09563102
ITGA10	-2.14628199	4.3992137	-4.43970856	0.0004854	0.04819688	0.06717436

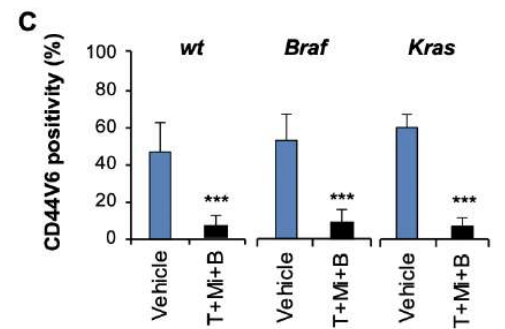
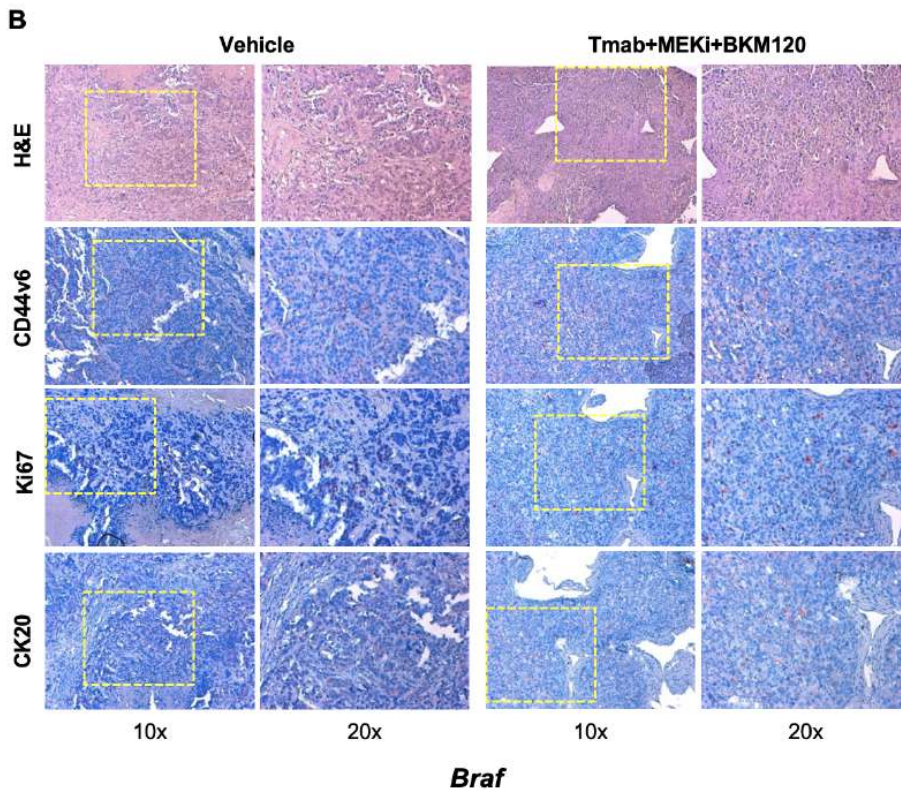
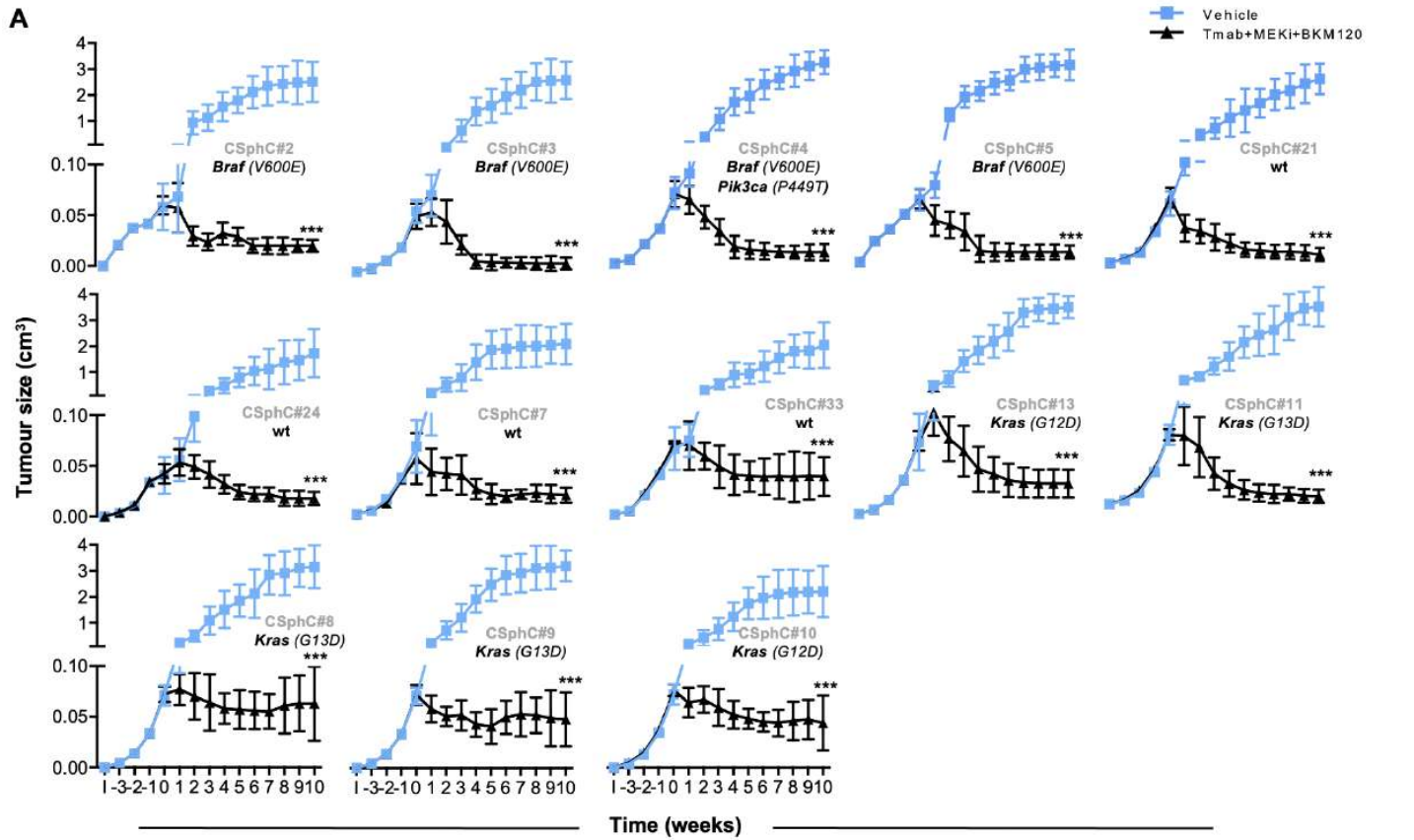


Supplementary Figure 3 Mangiapane et al.

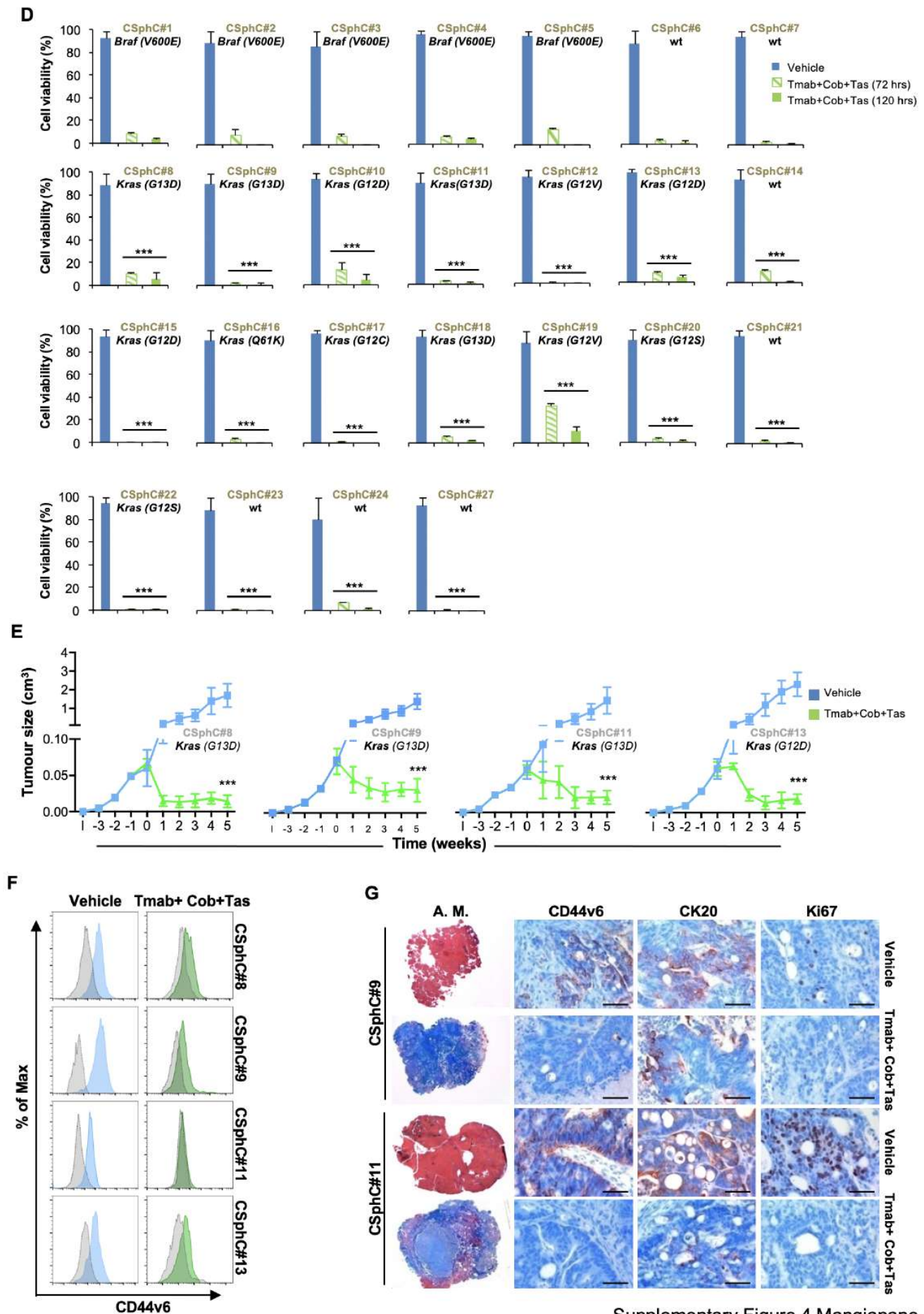


Supplementary Figure 3 Mangiapane et al.





Supplementary Figure 4 Mangiapane et al.



Supplementary Figure 4 Mangiapane et al.



Supplementary Table 4: RPPA antibody validation.

Validation Status*		*RPPA Set 131-Present*								
Valid = RPPA and WB correlation > 0.7										
Use with Caution = RPPA and WB correlation < 0.7										
Under Evaluation = Antibody has given mixed results and/or evaluated by another lab; We are in the process of (re)validating										
Used for QC = These antibodies are used for tissue sample quality control (QC); WILL NOT report to Datasets containing tissue samples, but WILL report to Datasets containing cell line samples										
#	Official Ab Name	Ab Name Reported on Dataset	Gene Name	Company	Catalog #	Internal Ab ID	Species	Validation Status*	RPPA Dilution	Storage
1	14-3-3 beta	14-3-3-beta	YWHA B	Santa Cruz	sc-628	882	Rabbit	Valid	1:75	4
2	14-3-3 epsilon	14-3-3-epsilon	YWHA E	Santa Cruz	sc-23957	913	Mouse	Use with Caution	1:50	4
3	14-3-3 zeta	14-3-3-zeta	YWHA Z	Santa Cruz	sc-1019	883	Rabbit	Valid	1:5000	4
4	4E-BP1	4E-BP1	EIF4EBP1	CST	9452	2	Rabbit	Valid	1:100	-20
5	4E-BP1 (phospho S65)	4E-BP1_pS65	EIF4EBP1	CST	9456	3	Rabbit	Valid	1:250	-20
6	53BP1	53BP1	TP53BP1	CST	4937	985	Rabbit	Valid	1:300	-20
7	Acetyl CoA Carboxylase (phospho S79)	ACC_pS79	ACACA, ACACB	CST	3661	13	Rabbit	Valid	1:500	-20
8	Acetyl CoA Carboxylase 1	ACC1	ACACA	Abcam	ab45174	14	Rabbit	Use with Caution	1:2000	-20
9	ADAR1	ADAR1	ADAR	Abcam	ab88574	1198	Mouse	Valid	1:200	-20
10	Akt	Akt	AKT1,2,3	CST	4691	1084	Rabbit	Valid	1:10000	-20
11	Akt (phospho S473)	Akt_pS473	AKT1,2,3	CST	9271	230	Rabbit	Valid	1:150	-20
12	Akt (phospho T308)	Akt_pT308	AKT1,2,3	CST	2965	1154	Rabbit	Valid	1:500	-20
13	AMPK alpha	AMPKa	PRKAA1	CST	2532	39	Rabbit	Use with Caution	1:200	-20
14	AMPK alpha (phospho T172)	AMPKa_pT172	PRKAA1	CST	2535	40	Rabbit	Use with Caution	1:100	-20
15	AMPK alpha 2 (Phospho S345)	AMPK-a2_pS345	PRKAA2	Abcam	ab129081	1351	Rabbit	Valid	1:500	-20
16	Androgen Receptor	AR	AR	Abcam	ab52615	756	Rabbit	Valid	1:100	-20
17	Annexin I	Annexin-I	ANXA1	BD Biosciences	610066	1208	Mouse	Valid	1:5000	-20
18	Annexin VII	Annexin-VII	ANXA7	BD Biosciences	610668	1142	Mouse	Valid	1:30	-20
19	A-Raf	A-Raf	ARAF	CST	4432	1217	Rabbit	Valid	1:150	-20
20	ARID1A	ARID1A	ARID1A	Sigma-Aldrich	HPA005456	1442	Rabbit	Use with Caution	1:1000	-20
21	Atg3	Atg3	ATG3	CST	3415	1612	Rabbit	Valid	1:750	-20
22	Atg7	Atg7	ATG7	CST	8558	1613	Rabbit	Valid	1:1000	-20
23	ATM	ATM	ATM	CST	2873	1363	Rabbit	Valid	1:250	-20
24	ATM (phospho S1981)	ATM_pS1981	ATM	CST	5883	1364	Rabbit	Valid	1:25	-20
25	ATR (Phospho S428)	ATR_pS428	ATR	Abcam	ab178407	1795	Rabbit	Use with Caution	1:1000	-20
26	ATRX	ATRX	ATRX	Abcam	ab97508	1569	Rabbit	Use with Caution	1:1000	-20
27	Aurora B/AIM1	Aurora-B	AIM1	CST	3094	1404	Rabbit	Valid	1:50	-20
28	Axl	Axl	AXL	CST	8661	1271	Rabbit	Valid	1:1000	-20
29	B7-H4	B7-H4	VTCN1	CST	14572	1726	Rabbit	Use with Caution	1:50	-20
30	Bad (phospho S112)	Bad_pS112	BAD	CST	9291	63	Rabbit	Valid	1:50	-20
31	Bak	Bak	BAK1	Abcam	ab32371	71	Rabbit	Use with Caution	1:30	-20
32	BAP1	BAP1	BAP1	Santa Cruz	sc-28383	1207	Mouse	Valid	1:125	4
33	Bax	Bax	BAX	CST	2772	73	Rabbit	Valid	1:100	-20
34	Bcl2	Bcl2	BCL2	Dako	M0887	80	Mouse	Valid	1:50	4
35	Bcl2A1	Bcl2A1	BCL2A1	Abnova	PAB8528	1299	Rabbit	Valid	1:250	-20
36	Bcl-xL	Bcl-xL	BCL2L1	CST	2762	85	Rabbit	Valid	1:100	-20
37	Beclin	Beclin	BECN1	Santa Cruz	sc-10086	87	Goat	Use with Caution	1:250	4
38	beta Actin	b-Actin	ACTB	CST	4970	1169	Rabbit	Use with Caution	1:75	-20
39	beta Catenin	b-Catenin	CTNNB1	CST	9562	75	Rabbit	Valid	1:1500	-20
40	beta Catenin (phospho T41/S45)	b-Catenin_pT41_S45	CTNNB1	CST	9565	1170	Rabbit	Valid	1:30	-20
41	Bid	Bid	BID	Abcam	ab32060	88	Rabbit	Use with Caution	1:30	-20
42	Bim	Bim	BCL2L11	Abcam	ab32158	90	Rabbit	Valid	1:400	-20
43	BIP/GRP78	BIP-GRP78	HSPA5	BD Biosciences	610978	1311	Mouse	Use with Caution	1:750	-20
44	B-Raf	B-Raf	BRAF	CST	14814	2083	Rabbit	Use with Caution	1:500	-20
45	B-Raf (phospho S445)	B-Raf_pS445	BRAF	CST	2696	94	Rabbit	Valid	1:1000	-20
46	BRD4	BRD4	BRD4	CST	13440	1567	Rabbit	Valid	1:200	-20
47	c-Abl	c-Abl	ABL	CST	2862	1565	Rabbit	Valid	1:50	-20
48	c-IAP2	c-IAP2	BIRC3	CST	3130	1615	Rabbit	Use with Caution	1:750	-20
49	Caspase-3 active	Caspase-3	CASP3	Abcam	ab32042	108	Rabbit	Use with Caution	1:250	-20
50	Caspase-7 (cleaved D198)	Caspase-7-cleaved	CASP7	CST	9491	109	Rabbit	Use with Caution	1:75	-20
51	Caspase-8	Caspase-8	CASP8	CST	9746	951	Mouse	**Used for QC**	1:150	-20
52	Caveolin-1	Caveolin-1	CAV1	CST	3238	114	Rabbit	Valid	1:5000	-20
53	CD171 (L1)	CD171	L1CAM	BioLegend	826701	1737	Mouse	Valid	1:1000	4
54	CD26	CD26	CD26	Abcam	ab28340	1308	Rabbit	Valid	1:1000	-20
55	CD29	CD29	ITGB1	BD Biosciences	610467	1206	Mouse	Valid	1:30	-20
56	CD31	CD31	PECAM1	Dako	M0823	127	Mouse	Valid	1:30	4
57	CD44	CD44	CD44	CST	3570	1398	Mouse	Use with Caution	1:50	-20
58	CD49b	CD49b	ITGA2	BD Biosciences	611016	937	Mouse	Valid	1:50	-20
59	cdc2 (Phospho Y15)	cdc2_pY15	CDK1	CST	4539	1783	Rabbit	Use with Caution	1:250	-20
60	cdc25C	cdc25C	CDC25C	CST	4688	1873	Rabbit	Valid	1:500	-20
61	CDK1	CDK1	CDK1	Abcam	ab32384	1658	Rabbit	Use with Caution	1:1000	-20
62	CDKN2A/p16INK4a	p16INK4a	CDKN2A	Abcam	ab81278	1231	Rabbit	Valid	1:500	-20
63	Chk1	Chk1	CHEK1	CST	2360	1203	Mouse	Use with Caution	1:250	-20
64	Chk1 (phospho S296)	Chk1_pS296	CHEK1	Abcam	ab79758	1348	Rabbit	Valid	1:125	-20
65	Chk2	Chk2	CHEK2	CST	3440	146	Mouse	Valid	1:50	-20
66	Chk2 (phospho T68)	Chk2_pT68	CHEK2	CST	2197	147	Rabbit	Use with Caution	1:125	-20
67	c-Jun (phospho S73)	c-Jun_pS73	JUN	CST	9164	155	Rabbit	Valid	1:30	-20
68	c-Kit	c-Kit	KIT	Abcam	ab32363	157	Rabbit	Valid	1:30	-20
69	Claudin 7	Claudin-7	CLDN7	Novus Biologicals	NB100-91714	852	Rabbit	Valid	1:300	-20
70	c-Met	c-Met	MET	CST	3127	726	Mouse	**Used for QC**	1:250	-20
71	c-Met (phospho Y1234/Y1235)	c-Met_pY1234_Y1235	MET	CST	3129	727	Rabbit	Valid	1:100	-20
72	c-Myc	c-Myc	MYC	Santa Cruz	sc-764	1143	Rabbit	Use with Caution	1:125	4
73	COG3	COG3	COG3	ProteinTech	11130-1-AP	1656	Rabbit	Valid	1:750	-20
74	COL6A1	Collagen-VI	COL6A1	Santa Cruz	sc-20649	171	Rabbit	Valid	1:5000	4
75	Connexin 43	Connexin-43	CN3A2	CST	3512	1568	Rabbit	Use with Caution	1:150	-20
76	Cox2	Cox2	PTGS2	CST	4842	1218	Rabbit	Use with Caution	1:50	-20
77	Cox-IV	Cox-IV	PTGS3	CST	4850	1116	Rabbit	Valid	1:1000	-20
78	C-Raf (phospho S338)	C-Raf_pS338	RAF1	CST	9427	179	Rabbit	Valid	1:100	-20



79	C-Raf/Raf-1	C-Raf	RAF1	Millipore	04-739	1201	Rabbit	Use with Caution	1:200	-20
80	CREB	CREB	CREB1	CST	9197	181	Rabbit	Use with Caution	1:1000	-20
81	Cyclin B1	Cyclin-B1	CCNB1	Epitomics	1495-1	192	Rabbit	Valid	1:1500	-20
82	Cyclin D1	Cyclin-D1	CCND1	Santa Cruz	sc-718	194	Rabbit	Valid	1:200	4
83	Cyclin D3	Cyclin-D3	CCND3	CST	2936	198	Mouse	Valid	1:1000	-20
84	Cyclin E1	Cyclin-E1	CCNE1	Santa Cruz	sc-247	201	Mouse	Valid	1:30	4
85	Cyclophilin F	Cyclophilin-F	PP1F	Abcam	ab110324	1257	Mouse	Valid	1:50000	4
86	Detyrosinated alpha-Tubulin	D- $\alpha$ -Tubulin	TUBA1A	Abcam	ab48389	1379	Rabbit	Valid	1:500	-20
87	Dimethyl-Histone H3 (Lys4)	DM-Histone-H3	HISTH3	Millipore	07-030	1380	Rabbit	Valid	1:1500	-20
88	Dimethyl-K9 Histone H3	DM-K9-Histone-H3	H3K9ME2	Abcam	ab32521	1397	Rabbit	Use with Caution	1:250	-20
89	DUSP4/MKP2	DUSP4	DUSP4	CST	5149	1406	Rabbit	Valid	1:250	-20
90	E2F-1	E2F1	E2F1	Santa Cruz	sc-251	1261	Mouse	Valid	1:30	4
91	E-Cadherin	E-Cadherin	CDH1	CST	3195	1099	Rabbit	Valid	1:300	-20
92	eEF2	eEF2	EEF2	CST	2332	1060	Rabbit	Use with Caution	1:50	-20
93	eEF2K	eEF2K	EEF2K	CST	3692	1061	Rabbit	Valid	1:50	-20
94	EGFR	EGFR	EGFR	CST	2232	1120	Rabbit	Valid	1:100	-20
95	EGFR (phospho Y1173)	EGFR_pY1173	EGFR	Abcam	ab32578	221	Rabbit	Valid	1:50	-20
96	eIF4E	eIF4E	EIF4E	CST	9742	722	Rabbit	Valid	1:75	-20
97	eIF4E (Phospho S209)	eIF4E_pS209	EIF4E	Abcam	ab76256	1871	Rabbit	Valid	1:500	-20
98	eIF4G	eIF4G	EIF4G1	CST	2498	1124	Rabbit	Use with Caution	1:1000	-20
99	Elk1 (phospho S383)	Elk1_pS383	ELK1	CST	9181	228	Rabbit	Use with Caution	1:50	-20
100	ENY2	ENY2	ENY2	GeneTex	GTX629542	1219	Mouse	Use with Caution	1:1000	-20
101	Epithelial Membrane Antigen	EMA	EMA	Dako	M061329-2	1350	Mouse	Use with Caution	1:1000	4
102	ErbB2/HER2	HER2	ERBB2	Lab Vision	MS-325-P1	1038	Mouse	Valid	1:3000	4
103	ErbB2/HER2 (phospho Y1248)	HER2_pY1248	ERBB2	R&D Systems	AF1768	1075	Rabbit	Use with Caution (likely sees pEGFR)	1:1500	-20
104	ErbB3/HER3	HER3	ERBB3	Santa Cruz	sc-285	911	Rabbit	Valid	1:300	4
105	ErbB3/HER3 (phospho Y1289)	HER3_pY1289	ERBB3	CST	4791	728	Rabbit	Use with Caution	1:50	-20
106	ERCC1	ERCC1	ERCC1	Santa Cruz	sc-17809	1357	Mouse	Valid	1:30	4
107	ERCC5	ERCC5	ERCC5	ProteinTech	11331-1-AP	1355	Rabbit	Use with Caution	1:250	-20
108	ERRF1/MIG6	MIG6	ERRF1	Sigma-Aldrich	WH0054206M1	1062	Mouse	Valid	1:50	-20
109	Estrogen Receptor	ER	ESR1	Lab Vision	RM-9101	238	Rabbit	Valid	1:40	4
110	Estrogen Receptor alpha (Phospho S118)	ER- $\alpha$ _pS118	ESR1	Abcam	ab32396	241	Rabbit	Valid	1:1000	-20
111	Ets-1	Ets-1	ETS1	Bethyl	A303-501A	1200	Rabbit	Valid	1:100	4
112	FAK	FAK	PTK2	Abcam	ab40794	252	Rabbit	Use with Caution	1:1000	-20
113	FAK (phospho Y397)	FAK_pY397	PTK2	CST	3283	1227	Rabbit	Valid	1:30	-20
114	Fatty Acid Synthase	FASN	FASN	CST	3180	1156	Rabbit	Valid	1:1000	-20
115	Fibronectin	Fibronectin	FN1	Epitomics	1574-1	262	Rabbit	Valid	1:10000	-20
116	FoxM1	FoxM1	FOXM1	CST	5436	1123	Rabbit	Valid	1:30	-20
117	FoxO3a	FoxO3a	FOXO3	CST	2497	1122	Rabbit	Use with Caution	1:25	-20
118	FoxO3a (phospho S318/S321)	FoxO3a_pS318_S321	FOXO3	CST	9465	270	Rabbit	Use with Caution	1:30	-20
119	FRA-1	FRA-1	FRA1	Santa Cruz	sc-605	1184	Rabbit	Use with Caution	1:100	4
120	G6PD	G6PD	G6PD	CST	8866	1779	Rabbit	Valid	1:1000	-20
121	Gab2	Gab2	GAB2	CST	3239	943	Rabbit	Valid	1:300	-20
122	GAPDH	GAPDH	GAPDH	Life Technologies	AM4300	274	Mouse	Use with Caution	1:50000	-20
123	GATA3	GATA3	GATA3	BD Biosciences	558686	764	Mouse	Valid	1:300	4
124	GCLM	GCLM	GCLM	Abcam	ab124827	1745	Rabbit	Use with Caution	1:500	-20
125	GCN5L2	GCN5L2	KAT2A	CST	3305	1263	Rabbit	Valid	1:30	-20
126	Glutamate Dehydrogenase1/2	Glutamate-D1-2	GLUD	CST	12793	1617	Rabbit	Use with Caution	1:500	-20
127	Glutaminase	Glutaminase	GLS	Abcam	ab156876	1491	Rabbit	Use with Caution	1:250	-20
128	Glycogen Synthase	Gys	GYS1	CST	3886	1035	Rabbit	Valid	1:1500	-20
129	Glycogen Synthase (phospho S641)	Gys_pS641	GYS1	CST	3891	1036	Rabbit	Valid	1:250	-20
130	Granzyme B	Granzyme-B	GZMB	CST	4275	1807	Rabbit	Valid	1:500	-20
131	GSK-3alpha/beta	GSK-3a-b	GSK3A, GSK3B	Santa Cruz	sc-7291	284	Mouse	Valid	1:750	4
132	GSK-3alpha/beta (phospho S21/S9)	GSK-3a-b_pS21_S9	GSK3A, GSK3B	CST	9331	285	Rabbit	Valid	1:200	-20
133	H2AX (phospho S140)	H2AX_pS140	H2AX	Pierce Biotechnology	MA1-2022	1409	Mouse	Use with Caution	1:400	-20
134	Heregulin	Heregulin	NRG1	CST	2573	890	Rabbit	Valid	1:30	-20
135	HES1	HES1	HES1	CST	11988	1582	Rabbit	Valid	1:1000	-20
136	Hexokinase II	Hexokinase-II	HK2	CST	2867	1023	Rabbit	Valid	1:50	-20
137	Hif-1 alpha	Hif-1-alpha	HIF1A	BD Biosciences	610958	1402	Mouse	Use with Caution	1:50	-20
138	Histone H3	Histone-H3	H3F3A, H3F3B	Abcam	ab1791	1250	Rabbit	Valid	1:3000	-20
139	HSP27	HSP27	HSP27	CST	2402	321	Mouse	Use with Caution	1:100	-20
140	HSP27 (phospho S82)	HSP27_pS82	HSBP1	CST	2401	323	Rabbit	Valid	1:75	-20
141	HSP70	HSP70	HSP70	CST	4872	325	Rabbit	Use with Caution	1:150	-20
142	IGF1R (phospho Y1135/Y1136)	IGF1R_pY1135_Y1136	IGF1R	CST	3024	1221	Rabbit	Valid	1:30	-20
143	IGFBP2	IGFBP2	IGFBP2	CST	3922	335	Rabbit	Valid	1:50	-20
144	IGFRb	IGFRb	INSR	CST	3027	336	Rabbit	Use with Caution	1:250	-20
145	INPP4b	INPP4b	INPP4B	CST	4039	1065	Rabbit	Valid	1:25	-20
146	Insulin Receptor beta	IR-b	INSRB	CST	3025	1586	Rabbit	Use with Caution	1:750	-20
147	IRF-1	IRF-1	IRF1	Santa Cruz	sc-497	1316	Rabbit	Use with Caution	1:200	4
148	IRS1	IRS1	IRS1	Millipore	06-248	802	Rabbit	Valid	1:400	-20
149	Jagged1	Jagged1	JAG1	Abcam	ab109536	1413	Rabbit	Valid	1:750	-20
150	Jak2	Jak2	JAK2	CST	3230	1166	Rabbit	Valid	1:750	-20
151	JNK/SAPK (phospho T183/Y185)	JNK_pT183_Y185	MAPK8	CST	4668	888	Rabbit	Valid	1:30	-20
152	JNK2	JNK2	MAPK9	CST	4672	380	Rabbit	Use with Caution	1:30	-20
153	LC3A/B	LC3A-B	LC3AB	CST	4108	1618	Rabbit	Use with Caution	1:500	-20
154	Lck	Lck	LCK	CST	2752	397	Rabbit	Valid	1:100	-20
155	LDHA	LDHA	LDHA	CST	3582	976	Rabbit	Use with Caution	1:250	-20
156	LRP6 (phospho S1490)	LRP6_pS1490	LRP6	CST	2568	1367	Rabbit	Valid	1:500	-20
157	MAPK (phospho T202/Y204)	MAPK_pT202_Y204	MAPK1, MAPK3	CST	4377	405	Rabbit	Valid	1:30	-20
158	Mcl 1	Mcl-1	MCL1	CST	5453	1222	Rabbit	Valid	1:100	-20
159	MDM2 (phospho S166)	MDM2_pS166	MDM2	CST	3521	1164	Rabbit	Valid	1:50	-20
160	MEK1	MEK1	MAP2K1	Abcam	ab32576	417	Rabbit	Valid	1:1500	-20
161	MEK1 (phospho S217/S221)	MEK1_pS217_S221	MAP2K1 MAP2K2	CST	9154	1076	Rabbit	Valid	1:50	-20
162	MERIT40 (Phospho S29)	MERIT40_pS29	BABAM1	CST	12110	1952	Rabbit	Valid	1:1000	-20
163	Merlin/NF2	Merlin	NF2	Novus Biologicals	22710002	1046	Rabbit	Use with Caution	1:250	-20
164	MIF	MIF	MIF	Santa Cruz	sc-20121	1323	Rabbit	Use with Caution	1:300	4
165	MMP2	MMP2	MMP2	CST	4022	435	Rabbit	Valid	1:75	-20



166	Mnk1	Mnk1	MKNK1	CST	2195	1005	Rabbit	Valid	1:1000	-20
167	Monocarboxylic Acid Transporter 4	MCT4	SLC16A4	Millipore	AB3314P	1633	Rabbit	Valid	1:500	-20
168	MSH6	MSH6	MSH6	Novus Biologicals	22030002	1063	Rabbit	Use with Caution	1:1000	-20
169	MSI2	MSI2	MSI2	Abcam	ab76148	1675	Rabbit	Use with Caution	1:4000	-20
170	mTOR	mTOR	MTOR	CST	2983	444	Rabbit	Valid	1:1000	-20
171	mTOR (phospho S2448)	mTOR_pS2448	MTOR	CST	2971	446	Rabbit	Use with Caution	1:50	-20
172	Myosin heavy chain 11	Myosin-11	MYH11	Novus Biologicals	21370002	1139	Rabbit	Valid	1:5000	-20
173	Myosin Ila (phospho S1943)	Myosin-lla_pS1943	MYH9	CST	5026	1160	Rabbit	Valid	1:1000	-20
174	Myt1	Myt1	MYT1	CST	4282	1803	Rabbit	Use with Caution	1:2000	-20
175	NAPSIN A	NAPSIN-A	NAPSA	Abcam	ab129189	1274	Rabbit	Use with Caution	1:150	-20
176	N-Cadherin	N-Cadherin	CDH2	CST	4061	452	Rabbit	Valid	1:30	-20
177	NDRG1 (phospho T346)	NDRG1_pT346	NDRG1	CST	3217	1126	Rabbit	Valid	1:100	-20
178	NDUFB4	NDUFB4	NDUFB4	Abcam	ab110243	1345	Mouse	Valid	1:30	4
179	NF-kappaB p65 (phospho S536)	NF-kB-p65_pS536	RELA	CST	3033	457	Rabbit	Use with Caution	1:30	-20
180	Notch1	Notch1	NOTCH1	CST	3268	1064	Rabbit	Valid	1:30	-20
181	Notch3	Notch3	NOTCH3	Santa Cruz	sc-5593	767	Rabbit	Use with Caution	1:300	4
182	N-Ras	N-Ras	NRAS	Santa Cruz	sc-31	1136	Mouse	Valid	1:50	4
183	Oct-4	Oct-4	OCT4	CST	2750	1669	Rabbit	Use with Caution	1:200	-20
184	p21	p21	CDKN1A	Santa Cruz	sc-397	470	Rabbit	Valid	1:150	4
185	p27 KIP 1	p27-Kip-1	CDKN1B	Abcam	ab32034	897	Rabbit	Valid	1:50	-20
186	p27/KIP 1 (phospho T198)	p27_pT198	CDKN1B	Abcam	ab64949	878	Rabbit	Valid	1:30	-20
187	p38 MAPK	p38	MAPK14	CST	9212	478	Rabbit	Valid	1:1500	-20
188	p38 MAPK (phospho T180/Y182)	p38_pT180_Y182	MAPK14	CST	9211	479	Rabbit	Valid	1:50	-20
189	p44/42 MAPK	p44-42-MAPK	MAPK3	CST	4695	1119	Rabbit	Valid	1:2000	-20
190	p53	p53	TP53	CST	9282	481	Rabbit	Use with Caution	1:2500	-20
191	p70 S6 Kinase (phospho T389)	p70-S6K_pT389	RPS6KB1	CST	9205	494	Rabbit	Valid	1:50	-20
192	p70/S6K1	p70-S6K1	RPS6KB1	Abcam	ab32529	493	Rabbit	Valid	1:300	-20
193	p90RSK (phospho T573)	p90RSK_pT573	RPS6K	CST	9346	1178	Rabbit	Use with Caution	1:30	-20
194	PAI-1	PAI-1	SERPINE1	BD Biosciences	612024	499	Mouse	Valid	1:100	-20
195	PAICS	PAICS	PAICS	Sigma-Aldrich	HPA035895	1322	Rabbit	Use with Caution	1:250	-20
196	PAK1	PAK1	PAK1	CST	2602	1811	Rabbit	Valid	1:1000	-20
197	PAK4	PAK4	PAK4	CST	3242	1389	Rabbit	Valid	1:750	-20
198	PAR	PAR	PAR	Trevigen	4336-BPC-100	1370	Rabbit	Use with Caution	1:15000	-20
199	PARK7/DJ1	DJ1	PARK7	Abcam	ab76008	891	Rabbit	Valid	1:5000	-20
200	PARP	PARP	PARP1	CST	9532	2185	Rabbit	Valid	1:1000	-20
201	Paxillin	Paxillin	PXN	Epitomics	1500-1	505	Rabbit	Use with Caution	1:500	-20
202	P-Cadherin	P-Cadherin	CDH3	CST	2130	509	Rabbit	Use with Caution	1:50	-20
203	PCNA	PCNA	PCNA	CST	2586	1383	Mouse	Use with Caution	1:1000	-20
204	Pdcd4	Pdcd4	PDCD4	Rockland	600-401-965	816	Rabbit	Use with Caution	1:750	-20
205	PDGFR beta	PDGFR-b	PDGFRB	CST	3169	1225	Rabbit	Valid	1:100	-20
206	PDHK1	PDHK1	PDHK1	CST	3820	1622	Rabbit	Use with Caution	1:500	-20
207	PDK1	PDK1	PDPK1	CST	3062	515	Rabbit	Valid	1:50	-20
208	PDK1 (phospho S241)	PDK1_pS241	PDPK1	CST	3061	516	Rabbit	Valid	1:50	-20
209	PD-1	PD-1	CD274	CST	13684	1724	Rabbit	Use with Caution	1:150	-20
210	PEA-15	PEA-15	PEA15	CST	2780	1017	Rabbit	Valid	1:100	-20
211	PED/PEA-15 (phospho S116)	PEA-15_pS116	PEA15	Invitrogen	44-836G	1018	Rabbit	Valid	1:1000	-20
212	PI3 Kinase p110 alpha	PI3K-p110-a	PIK3CA	CST	4255	808	Rabbit	Use with Caution	1:75	-20
213	PI3K p110 beta	PI3K-p110-b	PIK3CB	Santa Cruz	sc-376412	1330	Mouse	Use with Caution	1:60	4
214	PI3K p85	PI3K-p85	PIK3R1	Millipore	06-195	523	Rabbit	Valid	1:15000	-20
215	PKA RI alpha	PKA-a	PRKAR1A	CST	5675	1667	Rabbit	Valid	1:200	-20
216	PKCalpha	PKCa	PRKCA	CST	2056	1158	Rabbit	Valid	1:200	-20
217	PKC beta II (phospho S660)	PKC-b-II_pS660	PRKCA, PRKCB PRKCD, PRKCE PRKCH, PRKCQ	CST	9371	1137	Rabbit	Valid	1:200	-20
218	PKC delta (phospho S664)	PKC-delta_pS664	PRKCD	Millipore	07-875	932	Rabbit	Valid	1:100	-20
219	PKM2	PKM2	PKM2	CST	4053	1025	Rabbit	Use with Caution	1:300	-20
220	PLC gamma2 (phospho Y759)	PLC-gamma2_pY759	PLCG2	CST	3874	1030	Rabbit	Use with Caution	1:30	-20
221	PLK1	PLK1	PLK1	CST	4513	754	Rabbit	Use with Caution	1:125	-20
222	PMS2	PMS2	PMS2	Novus Biologicals	22510002	1246	Rabbit	Valid	1:1500	-20
223	PRAS40	PRAS40	AKT1S1	Invitrogen	AHO1031	738	Mouse	Use with Caution	1:250	-20
224	PRAS40 (phospho T246)	PRAS40_pT246	AKT1S1	Life Technologies	441100G	739	Rabbit	Valid	1:500	-20
225	PREX1	PREX1	PREX1	Abcam	ab102739	1204	Rabbit	Valid	1:150	-20
226	Progesterone Receptor	PR	PGR	Abcam	ab32085	549	Rabbit	Valid	1:50	-20
227	PTEN	PTEN	PTEN	CST	9552	566	Rabbit	Valid	1:500	-20
228	Rab11	Rab11	RAB11A,B	CST	3539	1083	Rabbit	Under Evaluation	1:30	-20
229	Rab25	Rab25	RAB25	CST	4314	1150	Rabbit	Valid	1:30	-20
230	Rad50	Rad50	RAD50	Millipore	05-525	987	Mouse	Valid	1:100	-20
231	Rad51	Rad51	RAD51	CST	8875	1262	Rabbit	Valid	1:30	-20
232	Raptor	Raptor	RPTOR	CST	2280	1128	Rabbit	Valid	1:300	-20
233	Rb	Rb	RB1	CST	9309	552	Mouse	**Used for QC**	1:100	-20
234	Rb (phospho S807/S811)	Rb_pS807_S811	RB1	CST	9308	557	Rabbit	Valid	1:500	-20
235	RBM15	RBM15	RBM15	Novus Biologicals	21390002	1138	Rabbit	Valid	1:5000	-20
236	Rheb	Rheb	RHEB	R&D Systems	MAB3426	847	Mouse	Use with Caution	1:75	-20
237	Rictor	Rictor	RICTOR	CST	2114	1129	Rabbit	Use with Caution	1:100	-20
238	Rictor (phospho T1135)	Rictor_pT1135	RICTOR	CST	3806	1130	Rabbit	Valid	1:200	-20
239	RIP	RIP	RIP	CST	4926	1624	Rabbit	Use with Caution	1:250	-20
240	Rock-1	Rock-1	ROCK1	Santa Cruz	sc-5560	1334	Rabbit	Use with Caution	1:1000	4
241	RPA32	RPA32	RPA32	CST	2208	1368	Rat	Use with Caution	1:500	-20
242	RPA32 (Phospho S4/S8)	RPA32_pS4_S8	RPA32	Bethyl	A300-245A	1375	Rabbit	Use with Caution	1:250	4
243	RSK	RSK	RPS6KA1 RPS6KA2 RPS6KA3	CST	9347	759	Rabbit	Use with Caution	1:150	-20
244	S6 (phospho S235/S236)	S6_pS235_S236	RPS6	CST	2211	600	Rabbit	Valid	1:2500	-20
245	S6 (phospho S240/S244)	S6_pS240_S244	RPS6	CST	2215	601	Rabbit	Valid	1:1000	-20
246	S6 Ribosomal Protein	S6	RPS6	CST	2317	1874	Mouse	Valid	1:1000	-20
247	SCD	SCD	SCD	Santa Cruz	sc-58420	1127	Mouse	Valid	1:30	4
248	SDHA	SDHA	SDHA	CST	11998	1339	Rabbit	Valid	1:250	-20
249	SF2/ASF	SF2	SRSF1	Invitrogen	32-4500	1131	Mouse	Valid	1:150	-20
250	Shc (phospho Y317)	Shc_pY317	SHC1	CST	2431	1031	Rabbit	Valid	1:30	-20

251	SHP-2 (phospho Y542)	SHP-2_pY542	PTPN11	CST	3751	1180	Rabbit	Use with Caution	1:75	-20
252	SLC1A5	SLC1A5	SLC1A5	Sigma-Aldrich	HPA035240	1313	Rabbit	Use with Caution	1:15000	-20
253	Sfn11	Sfn11	SLFN11	Santa Cruz	sc-136891	1411	Goat	Use with Caution	1:250	4
254	Smac/Diablo	Smac	DIABLO	CST	2954	610	Mouse	**Used for QC**	1:150	-20
255	Smad1	Smad1	SMAD1	Abcam	ab33902	922	Rabbit	Valid	1:750	-20
256	Smad3	Smad3	SMAD3	Abcam	ab40854	796	Rabbit	Valid	1:150	-20
257	Smad4	Smad4	SMAD4	Santa Cruz	sc-7966	920	Mouse	Valid	1:30	4
258	Snail	Snail	SNAI1	CST	3895	616	Mouse	**Used for QC**	1:50	-20
259	SOD1	SOD1	SOD1	CST	4266	1818	Mouse	Valid	1:500	-20
260	SOD2	SOD2	SOD2	CST	13141	1328	Rabbit	Valid	1:2500	-20
261	Sox2	Sox2	SOX2	CST	2748	1670	Rabbit	Valid	1:200	-20
262	Src	Src	SRC	Millipore	05-184	621	Mouse	Valid	1:200	-20
263	Src (phospho Y527)	Src_pY527	SRC, YES1, FYN FGR	CST	2105	626	Rabbit	Valid	1:30	-20
264	Src Family (phospho Y416)	Src_pY416	SRC, LYN, FYN LCK, YES1, HCK	CST	2101	623	Rabbit	Valid	1:500	-20
265	Stat3	Stat3	STAT3	CST	4904	1197	Rabbit	Use with Caution	1:3000	-20
266	Stat3 (phospho Y705)	Stat3_pY705	STAT3	CST	9131	637	Rabbit	Valid	1:30	-20
267	Stat5a	Stat5a	STAT5A	Abcam	ab32043	638	Rabbit	Valid	1:250	-20
268	Stathmin 1	Stathmin-1	STMN1	Abcam	ab52630	718	Rabbit	Valid	1:75	-20
269	Syk	Syk	SYK	Santa Cruz	sc-1240	1033	Mouse	Valid	1:3000	4
270	Tau	Tau	TAU	Millipore	05-348	646	Mouse	Use with Caution	1:100	-20
271	TAZ	TAZ	WWTR1	CST	4883	1848	Rabbit	Valid	1:300	-20
272	TFAM	TFAM	TFAM	CST	7495	1333	Rabbit	Valid	1:300	-20
273	TIGAR	TIGAR	C12ORF5	Abcam	ab137573	1107	Rabbit	Valid	1:100	-20
274	Transferrin Receptor	TFRC	TFRC	Novus Biologicals	22500002	1140	Rabbit	Valid	1:15000	-20
275	Transglutaminase II	Transglutaminase	TGM2	Lab Vision	MS-224-P1	908	Mouse	Valid	1:150	4
276	TRIM25	TRIM25	TRIM25	Abcam	ab167154	1756	Rabbit	Use with Caution	1:2000	-20
277	TSC1/Hamartin	TSC1	TSC1	CST	4906	1125	Rabbit	Use with Caution	1:200	-20
278	TSC2/Tuberin (phospho T1462)	Tuberin_pT1462	TSC2	CST	3617	671	Rabbit	Valid	1:30	-20
279	TTF1	TTF1	NKX2-1	Abcam	ab76013	1081	Rabbit	Valid	1:30	-20
280	Tuberin	Tuberin	TSC2	Abcam	ab32554	670	Rabbit	Valid	1:2500	-20
281	TUFM	TUFM	TUFM	Abcam	ab173300	1842	Rabbit	Valid	1:300	-20
282	Twist	TWIST	TWIST2	Santa Cruz	sc-81417	1353	Mouse	Use with Caution	1:30	4
283	Tyro3	Tyro3	TYRO3	CST	5585	1080	Rabbit	Valid	1:30	-20
284	UBAC1	UBAC1	UBAC1	Sigma-Aldrich	HPA005651	1270	Rabbit	Valid	1:250	-20
285	Ubiquitinyl Histone H2B	Ubq-Histone-H2B	H2BFM	Millipore	05-1312	1604	Mouse	Use with Caution	1:500	4
286	UGT1A	UGT1A	UGT1A1	Santa Cruz	sc-271268	1267	Mouse	Valid	1:75	4
287	ULK1 (phospho S757)	ULK1_pS757	ULK1	CST	6888	1626	Rabbit	Use with Caution	1:1000	-20
288	VASP	VASP	VASP	CST	3112	678	Rabbit	Valid	1:250	-20
289	VDAC1/Porin	Porin	VDAC1	Abcam	ab14734	1254	Mouse	Valid	1:300	-20
290	VEGF Receptor 2	VEGFR-2	KDR	CST	2479	688	Rabbit	Valid	1:12000	-20
291	VHL/EPPK1**	VHL-EPPK1	EPPK1	BD Biosciences	556347	693	Mouse	Under Evaluation (Targets EPPK1)	1:1000	4
292	Vimentin	Vimentin	VIM	Dako	M0725	1393	Mouse	Use with Caution	1:250	4
293	Wee1	Wee1	WEE1	CST	4936	1802	Rabbit	Use with Caution	1:2000	-20
294	Wee1 (Phospho S642)	Wee1_pS642	WEE1	CST	4910	2058	Rabbit	Use with Caution	1:75	-20
295	WIPI1	WIPI1	WIPI1	CST	12124	1627	Rabbit	Use with Caution	1:1000	-20
296	WIPI2	WIPI2	WIPI2	CST	8567	1628	Rabbit	Use with Caution	1:1000	-20
297	XBP1	XBP1	XBP1	Santa Cruz	sc-32136	1044	Goat	Use with Caution	1:200	4
298	XPA	XPA	XPA	Santa Cruz	sc-56813	1359	Mouse	Valid	1:75	4
299	XPF	XPF	XPF	Abcam	ab73720	2015	Rabbit	Use with Caution	1:100	-20
300	XRCC1	XRCC1	XRCC1	CST	2735	906	Rabbit	Use with Caution	1:30	-20
301	YAP	YAP	YAP1	Santa Cruz	sc-15407	780	Rabbit	Under Evaluation	1:200	4
302	YAP (phospho S127)	YAP_pS127	YAP1	CST	4911	782	Rabbit	Under Evaluation	1:750	-20
303	YB1 (phospho S102)	YB1_pS102	YBX1	CST	2900	835	Rabbit	Valid	1:50	-20
304	ZAP-70	ZAP-70	ZAP70	CST	2705	1828	Rabbit	Use with Caution	1:1000	-20